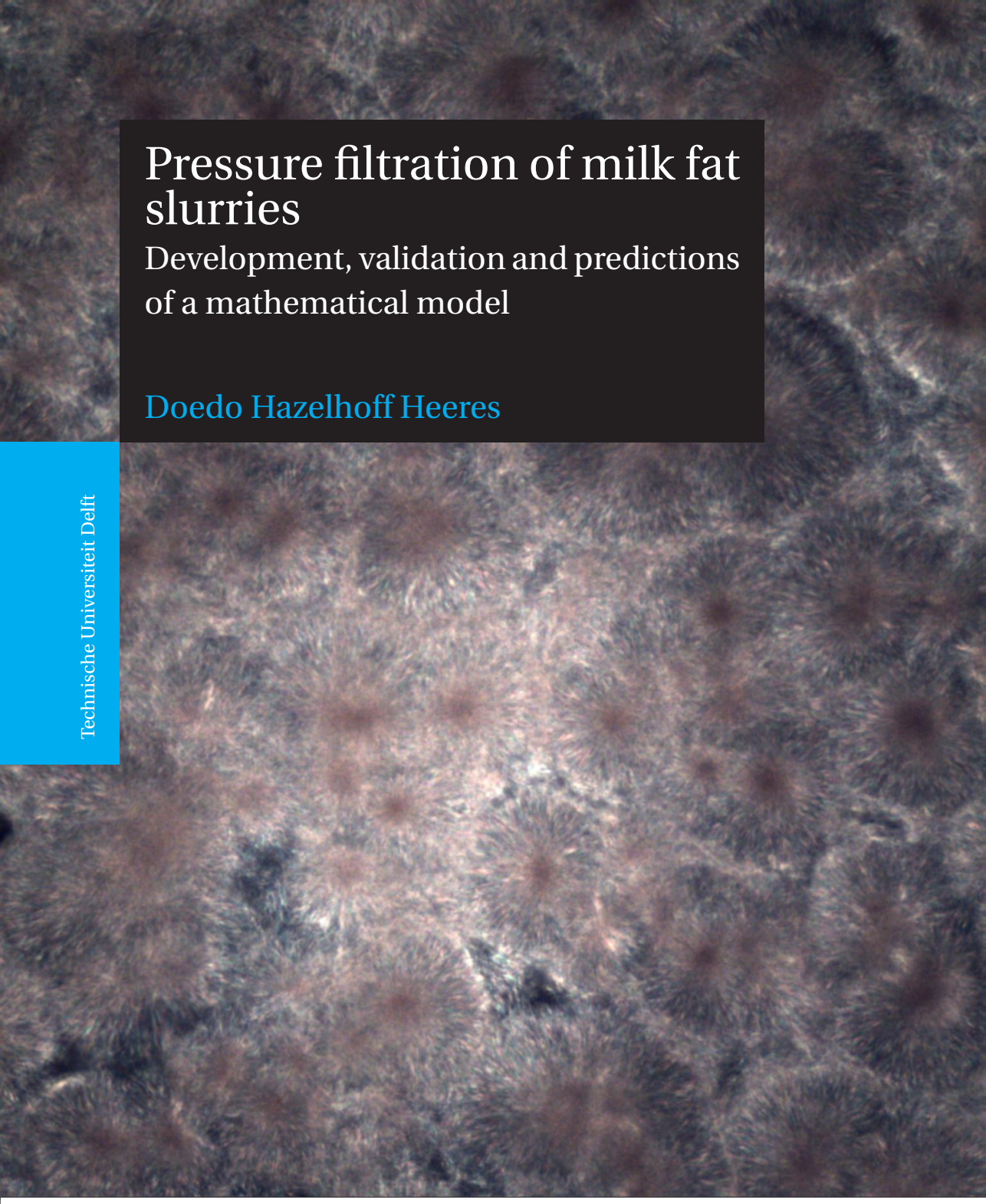

Pressure filtration of milk fat slurries

Development, validation and predictions of a mathematical model

Doedo Hazelhoff Heeres

Technische Universiteit Delft

TU Delft Delft University of Technology

Challenge the future

PRESSURE FILTRATION OF MILK FAT SLURRIES

DEVELOPMENT, VALIDATION AND PREDICTIONS OF A MATHEMATICAL MODEL

by

Doedo Philippus Hazelhoff Heeres

in partial fulfillment of the requirements for the degree of

Master of Science
in Applied Physics

at the Delft University of Technology,
to be defended publicly on Tuesday June 19, 2018 at 2:00 PM.

Student number:	1234420	
Project duration:	Januari 2, 2017 – June 14, 2018	
Thesis committee:	Prof. dr. ir. H. E. A. van den Akker,	TU Delft, supervisor
	Prof. dr. ir. C. R. Kleijn,	TU Delft
	Dr. ir. F. J. Vermolen,	TU Delft
	Dr. Ing. W. Kloek,	FrieslandCampina, supervisor

Cover design: Microscopical image of a slurry of milk fat crystal aggregates, typically with a diameter of 200 micrometer, taken by Doedo Hazelhoff Heeres in a laboratory of the FrieslandCampina Innovation Centre in Wageningen.

An electronic version of this thesis is available at http://repository.tudelft.nl/.

TU Delft Delft University of Technology

ABSTRACT

In this study, a pressure filtration model for a slurry of milk fat crystal aggregates is developed, validated and used to investigate the effect of pressure-time profiles. The model focuses on the expression step and describes oil flow locally. The filter cake is modelled as a double porous non-linear elastic medium with permeabilities described by the relation of Meyer & Smith. Conservation equations lead to a coupled system of differential equations, which are numerically solved exploiting a finite-difference scheme.
Simulations with the model give insight through graphs of volume fractions versus filter chamber location at any given time step. Diagrams of oil outflow velocities and solid fat content of produced filter cakes show qualitatively good behaviour when compared to experiments.
Studying the effect of pressure-time profiles, the model predicts that a low rate of pressure increase gives the driest filter cakes. Simulations also indicate that putting steps in pressure-time profiles is hardly effective.

CONTENTS

1

Introduction

When the gods performed the sacrifice,
with the first Man as the offering,
spring was the clarified butter,
summer the fuel,
autumn the oblation.

They anointed the Man,
the sacrifice born at the beginning,
upon the sacred grass.
With him the gods, Sadhyas,
and sages sacrificed.

From that sacrifice in which everything was offered,
the melted fat was collected,
and he made it into those beasts who live in the air,
in the forest,
and in villages.

The Rigveda, Mandala 10, ca 1200 BCE [1]

1

DAIRY is as old as the first agricultural revolution. The *Dey* in dairy is thought to have a root meaning *to knead bread*, pointing to squeezing buttermilk out of butter and whey out of cheese [2]. Pressure filtration is in that sense part of the essence of dairy.
To better understand the relation between pressure filtration and dairy, this introduction starts with a general introduction into filtration. After that, the benefits of butter are briefly discussed and this is followed by a short description of the production process of milk fat fractions. Next, a literature review and scope of this thesis is presented. The introduction is concluded with an outline of the thesis.

1.1. GENERAL INTRODUCTION TO FILTRATION

Filtration is a process in which a solid-liquid mixture is separated through a semi-permeable material that retains the solids and conducts the liquid (see figure 1.1). The liquid that is passed through is known as filtrate. Filtration can be seen in many different processes throughout the world in industry, in biological systems and so forth. For example, kidneys clean our blood by filtering it. In addition, one can think of preparing food and beverages in the kitchen. Making coffee or preparing pasta usually involves filtration.

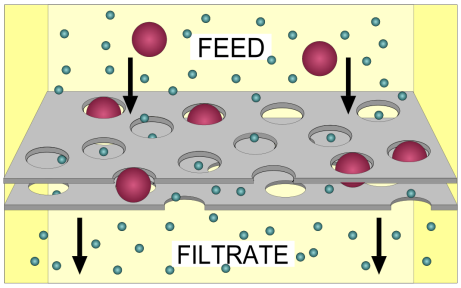

Figure 1.1: Filtration is a process in which a solid-liquid mixture, the feed, is separated through a semi-permeable material that retains the solids, while the liquid passes through as filtrate.

If the particles are larger than the pores of the filter medium, a filter cake will form on the filter medium. Therefore, this type of filtration is known as cake filtration[3]. In turn, pressure filtration is a form of cake filtration where the filter cake is squeezed out in the final stage to retrieve more liquid from the solid-liquid mixture, thereby attaining a better separation. This press step, also known as expression step, is often done using a pump which creates a positive pressure above the semi-permeable separating surface[4]. A filter press usually processes suspensions in a batch-wise manner. Pressure filtration serves a wide range of chemical and process industries. It is the right technique to use for suspensions that contain fine particles that settle slowly or when the solid content of the feed is high[4]. Examples where pressure filtration is utilised include:

- Dewatering of waste water sludge in waste water treatment[5],
- Thickening of minerals tailings in the mining industry[6], and
- Expression of biological material such as sugar beet pulp in the food industry[7].

The membrane filter press with compressible filter chambers was developed in the early 1980s for processing palm oil[8]. It is treated in more detail in section 2.1.
Pressure filtration is the subject of this thesis and to this day it is the preferred separation method for producing edible oil fractions[8].

Figure 1.2: The membrane filter press.

1.2. BUTTER, A CHEF'S GOLDMINE

Butter and other milk fat-based products are valuable products for the dairy industry due to their unique taste, their textural characteristics, and nutritional value[9]. For the same reasons they are indispensable ingredients in a chef's kitchen. Furthermore, milk fat is lauded for its reputation as a natural product[10].
Triglycerides, more commonly known as fats, are esters from three fatty acids and glycerol. Milk fat is the most complex natural fat[11]. It can be composed of a large variety of fatty acids and has a wide melting range. Dry fractionation, also known as melt crystallisation, is a physical separation process that can select milk fat components according to melting temperatures[10]. This enables to produce milk fat fractions with different functionalities. The liquid fraction is called olein fraction. The solid fraction, that can still contain part of the liquid, is called stearin fraction. Olein fractions are used for their structural, nutritional and sensorial functionalities. Examples include ice cream and butter that is spreadable at refrigerator temperature. The stearin fractions are mainly used for structural functionalities. One can think of specialty butters for the bakery, delivering extra crunchy croissant crusts adding to a better mouth feel. In chocolate it is used to act as an anti blooming agent.
Improving separation results in improved functionalities of milk fat fractions, creating more value for dairy companies. This thesis focuses on improving separation efficiency.

1.3. PRODUCTION PROCESS OF MILK FAT FRACTIONS

The production process starts with cattle in the meadow eating grass, ruminating and producing milk. The milk is collected from which the cream is skimmed. The cream is centrifuged undergoing a phase inversion process reaching a fat content of nearly 100 %. The resulting substance is named anhydrous milk fat (AMF), better known to chefs as clarified butter. The AMF is then separated using dry fractionation into an olein

(O) and a stearin (S) fraction.
Dry fractionation comprises two steps: crystallisation and pressure filtration. In the crystallisation process the AMF is completely melted at 60°C and then cooled down in a slowly stirred batch crystallizer according to a specific temperature profile that typically takes a quarter of a day. In this slow process, fat crystals nucleate and grow, eventually forming spherulitic aggregates that have a diameter of 100 µm in order of magnitude. The result is a slurry of fat crystal aggregates in oil (see figure 1.3), which is pressure filtrated using a particular pressure-time profile in a membrane filter press separating olein from stearin.

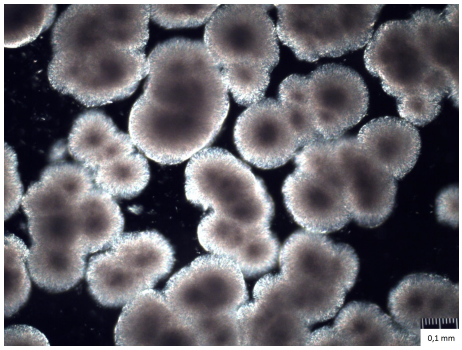

Figure 1.3: Microscopical image of the slurry with the milk fat crystal aggregates. In the bottom right corner, the 0.1 mm graphic scale is depicted.

Dry fractionation can be repeated on the O and S fractions in a multistep fractionation to create higher order O and S fractions like OO, OOO or SS fractions, all with different (melting) characteristics which can be useful in food products. With these fractions the problem can arise that the produced filter cake is too wet, which constitutes a product of poor quality that cannot be used or sold to costumers.
It is the purpose of this thesis and the model presented to give insights paving the way for solutions to this problem.

Some remarks about word use in this thesis: the words *olein* and *O fraction* will be strictly reserved for the filtrate, i.e. the oil that has been separated. The liquid phase that has not been separated will be denoted *oil* or simply as *liquid (phase)*. The words *stearin* and *S fraction* will be used for the filter cake when the press step is finished.

1.4. LITERATURE REVIEW

Ruth formulated the basic filtration equations still in use today. His equations relate filtrate volume as function of time to pressure drop over the filter cake and filter medium combined. These equations are based on filter cake averaged quantities such as specific resistance and filter cake volume[12].
Carman was the first to take filter cake structure into account relating its porosity to permeability[13]. Tiller et al. developed the conventional cake theory which combines

Darcy's law for the flow through porous media with the notion of a solid pressure[14]. This combination yields a diffusion equation with a diffusion coefficient that is named *(modified) consolidation coefficient.* It was first used by Terzaghi to model the consolidation of soils[15]. It is also in the field of soil mechanics that the concept of solid pressure finds its origin. Solid pressure is the accumulated average normal stress on the filter cake due to drag caused by liquid flow. Shirato expanded the Terzaghi model based on Voigt's notion of secondary consolidation to account for creep effects of the solid[16].

More recently, the work by Buttersack presented a simple approach to predict outcomes in pressure filtration of biological material requiring only three material specific parameters [17]. His model revolves around a threshold value for the void ratio, for which an elastic network is formed. This elastic network can be associated with dense sphere packings for a filter cake composed of spherical particles. The threshold value defines two zones, instead of chronological periods, that differentiate filtration from expression. Lanoisellé's paper on pressure filtration of cellular material is of interest as he recognises and implements different volumes in the filter cake[18]. He describes having a double porous medium which can account for flow from intraparticle to extraparticle volume and differences in flow resistance. He points out, that for cellular filter cakes the expression step is much more complex than for mineral cakes. The same might hold for filter cakes composed of AMF fat crystal aggregates. The *Liquid-Containing Biporous Particles Expression Model* shows promising results in comparison to the more classical Terzaghi-Voight and Terzaghi models. The paper by Petryk and Vorobiev uses a similar model to describe the expression of soft plant materials[19]. However, in both papers, the studied material and the applied pressures are very different from the ones subject in the present thesis.
A couple of papers dealing with pressure filtration of a material very similar to AMF were written by Kamst[20, 21]. Both papers deal with the expression of palm oil filter cakes. Kamst incorporates viscoelastic models from soil mechanics into his expression model. Nutting's non-linear viscoelastic model was originally designed to model asphalt and pitch[22]. In Kamst's modified form, it shows good correspondence with experiments [20]. Also, he reports good agreements with experiments using another non-linear viscoelastic model that takes into account the pressure history of the filter cake: the strain hardening model. He uses this model together with an empirical relation for the permeability in an expression model. Numerical implementation is done with a finite-difference scheme exploiting an exponential grid and a variable time step. Kamst's expression model predicts a pressure of 4.7 bar above which the solid fat content *(SFC)* does not increase[23]. He reports that constant pressure profiles in comparison with time-dependent pressure profiles with the same end pressure do not lead to a higher eventual *SFC* [24]. However, he did not compare different pressure-time profiles. The current thesis provides in the need for this comparison.
Some of Kamst's experiments and simulations exceed time scales that are relevant for the current thesis by an order of magnitude. In pursuit of finding a model for cake permeability, he discards the Kozeny-Carman equation[25]. However, it can be questioned whether Kamst uses the right porosity to draw this conclusion, as he ignores the double porous nature of the palm oil filter cake.

1

1.5. SCOPE OF THIS THESIS

The present thesis utilises Lanoisellé's concept of the double porous medium to study whether it can successfully model the expression of AMF filter cakes. Simulations based on the model are used to investigate the effect of different pressure-time profiles on the eventual *SFC*.

The overall goals of this thesis are:

- To develop a pressure filtration model and to write the computer code to perform numerical simulations.
- To validate the pressure filtration model.
- To perform simulations to gain insight into critical factors that lead to a higher olein yield.

Specific questions that will be addressed are:

- Is it favourable to apply a high rate of pressure increase in the pressure-time profile during the expression of AMF?
- Given a certain rate of pressure increase, does a one-step linear pressure-time profile give the highest eventual *SFC*?

These questions will be answered by using the pressure filtration model developed in this thesis.

1.6. OUTLINE OF THE THESIS

To create a firm foundation, the thesis will continue in chapter 2 with the *Theoretical background*. Here, it is explained how the membrane filter press operates, concepts as volume fraction, flow resistance, sphere packing and strain are introduced and governing equations are formulated. Chapter 3 formulates the novel *Pressure filtration model*. One of the important elements of the model is that the aggregates are regarded as sources for oil, when squeezed. Chapter 4 follows with a *Numerical implementation* of this model. The finite-difference scheme will be treated and it is shown how the behaviour near the boundary can be adequately dealt with. Next, the *Results* of comparisons of the model with experiments and results of simulations to investigate different pressure-time profiles will be presented in chapter 5. Chapter 6 completes this thesis with the *Conclusions and recommendations*.

2

THEORETICAL BACKGROUND

In this chapter the theoretical foundation is established for this thesis. First, the apparatus on which pressure filtration of milk fat fractions is performed is presented. Then, some geometrical definitions are given after which the governing equations for the filter cake are formulated. This is followed by the concept of flow resistance and experimental relations for permeability. A description of deformation concludes this theoretical background.

2.1. THE MEMBRANE FILTER PRESS

A membrane (plate) filter press, also known as diaphragm filter press, is composed of vertical plates which can slide on a rail with two layers of filter cloth in between (see figure 2.1). Stationary plates alternate with plates with a membrane that encloses a compression chamber on each side of the membrane plates. The plates form circa 3 cm thick filter chambers when they are held together with a thrust cylinder. The slurry is fed from the crystallisation tank into the filter chambers through a central pipe (see figure 2.2). This is referred to here as the *filling mode*. In this mode most of the filtrate is produced. When the filter chambers are full with crystal mass, the compression chambers are filled with air or water squeezing the filter cakes to push out more oil. This *pressing mode* is usually done with a prescribed pressure-time profile allowing the oil to flow through the pores of the filter cake.
The operation is finalised by blowing nitrogen through the pipes releasing the last oil, core cleaning and a cake discharge when the filter plates are taken apart which opens the filter chambers.
Cleaning the filter press and its filter cloth is usually done by rinsing it with warm oil.

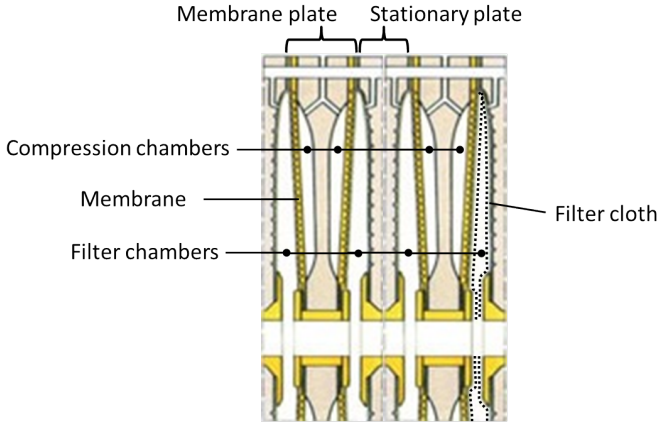

Figure 2.1: One membrane plate and one stationary plate are indicated. When held together, they seal off a filter chamber. The membranes separate the filter chambers from the compression chambers. In the filter chamber on the right, the location of the two filter cloths is indicated. (Modified version of [26]).

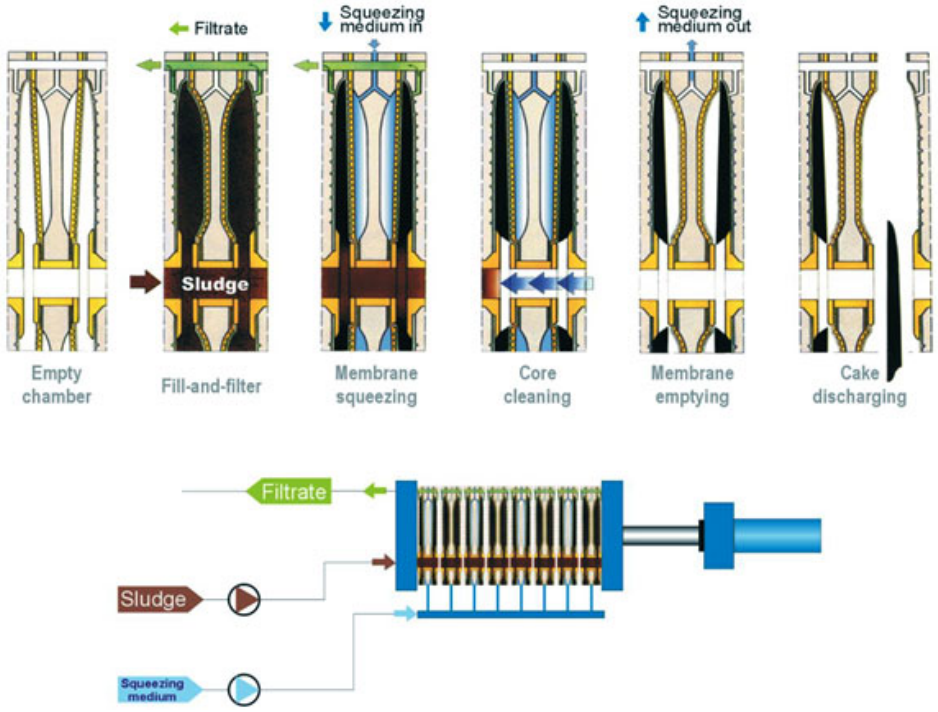

Figure 2.2: Sludge (slurry) is fed through a central pipe filling the filter chambers. As the squeezing medium is pumped inside, the membranes express the filter cakes. After core cleaning and membrane emptying, the cakes can be discharged. (Image taken from [26]).

2.2. VOLUME FRACTIONS OF A DOUBLE POROUS FILTER CAKE

The fat crystal aggregates in the process under consideration are spherulitic. Therefore, a filter cake composed of these aggregates resembles a mono-disperse sphere packing. The aggregate packing has pores that constitute the volume between the aggregates, the interaggregate volume. The aggregates are also porous and consist of fat crystals and oil. The pores of the aggregates are smaller by at least an order of magnitude compared to the interaggregate pores, which justifies referring to the filter cake as a double porous medium. A similar division of volumes and similar definitions treated in this section can be found in the paper of Lanoisellé et al [18].
Four different volumes can be distinguished in a fragment of filter cake with total volume $\delta V(t)$ which is depicted in figure 2.3:

1. Interaggregate volume δV_{ia};
2. Aggregate volume δV_a;
3. Aggregate pore volume δV_{ap};
4. Solid fat volume δV_s;

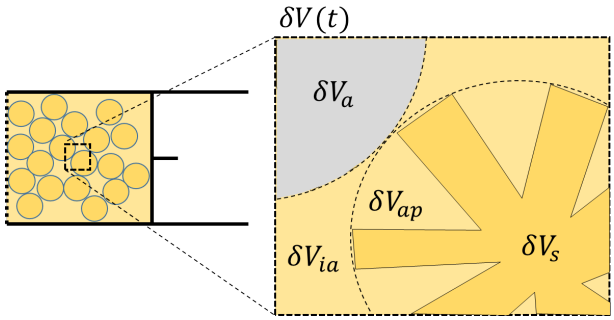

Figure 2.3: Identification of different volumes within a fragment of filter cake. δV_{ia} and δV_a sum up to δV. δV_a consists of δV_{ap} and δV_s.

The interaggregate volume and aggregate volume sum up to the total volume:

$$\delta V = \delta V_{ia} + \delta V_a. \tag{2.1}$$

The aggregate volume is composed of aggregate pore volume and solid fat volume such that:

$$\delta V_a = \delta V_{ap} + \delta V_s. \tag{2.2}$$

Dimensionless volumes such as the interaggregate porosity ε_1 and the aggregate porosity ε_2 are defined as follows:

$$\varepsilon_1 \equiv \frac{\delta V_{ia}}{\delta V}, \quad \varepsilon_2 \equiv \frac{\delta V_{ap}}{\delta V_a}. \tag{2.3}$$

The volume fraction complements, i.e. the interaggregate solidosity s_1 and the aggregate solidosity s_2, are formulated in a similar fashion:

$$s_1 \equiv \frac{\delta V_a}{\delta V} = 1 - \varepsilon_1, \quad s_2 \equiv \frac{\delta V_s}{\delta V_a} = 1 - \varepsilon_2. \tag{2.4}$$

The total solidosity (s), i.e. the solid fat volume fraction, is written as:

$$s \equiv \frac{\delta V_s}{\delta V} = s_1 s_2. \tag{2.5}$$

Another ratio of volumes that is commonly found in filtration literature is the void ratio. The following definitions of the interaggregate void ratio e_1 and aggregate void ratio e_2 are used in this thesis:

$$e_1 \equiv \frac{\delta V_{ia}}{\delta V_a} = \frac{\varepsilon_1}{s_1}, \quad e_2 \equiv \frac{\delta V_{ap}}{\delta V_s} = \frac{\varepsilon_2}{s_2}. \tag{2.6}$$

In parallel, the total void ratio is defined as:

$$e \equiv \frac{\delta V_{ia} + \delta V_{ap}}{\delta V_s}. \tag{2.7}$$

2.3. GOVERNING EQUATIONS

In this section the conservation of mass and momentum are formulated for both the solid phase and the interaggregate liquid phase to develop multiple useful relations.

2.3.1. CONSERVATION OF MASS

Mass conservation for the solid phase can be formulated as follows [27]:

$$\frac{\partial(s\rho_s)}{\partial t} + \vec{\nabla} \cdot (s\rho_s \vec{v}_s) = 0. \tag{2.8}$$

Here, ρ_s and $\vec{v}_s$ are the density and the velocity of the solid phase respectively.
Integration over a filter cake fragment with a volume $\delta V(t) = \delta x(t) \cdot \delta y \cdot \delta z$ (see figure 2.4), applying both Gauss's theorem and Leibniz–Reynolds transport theorem [28], leads to:

$$\frac{\mathrm{d}}{\mathrm{d}t} \int_{\delta V(t)} s\rho_s \mathrm{d}V = 0. \tag{2.9}$$

Considering $\delta V(t) \gg V_p$, where V_p is the typical pore volume, taking the 1D geometry encountered in the membrane plate filter press into account and assuming ρ_s constant, equation 2.9 reduces to:

$$\frac{\mathrm{d}}{\mathrm{d}t} \int_{\delta x(t)} s\mathrm{d}x = 0. \tag{2.10}$$

This should hold for any slice thickness $\delta x(t)$ so that:

$$\mathrm{d}\omega \equiv s\mathrm{d}x = \text{constant}, \tag{2.11}$$

defining the infinitesimal 1D solid volume dω. Equation 2.11 also expresses a transformation of coordinates $x \mapsto \omega$ that will be used in this thesis.

Analogously, taking ρ_l as the density of the liquid, conservation of interaggregate liquid mass is formulated as [27]:

$$\frac{\partial(\varepsilon_1 \rho_l)}{\partial t} + \vec{\nabla} \cdot (\varepsilon_1 \rho_l \vec{v}_l) = 0, \tag{2.12}$$

where the velocity of the liquid is denoted $\vec{v}_l$.

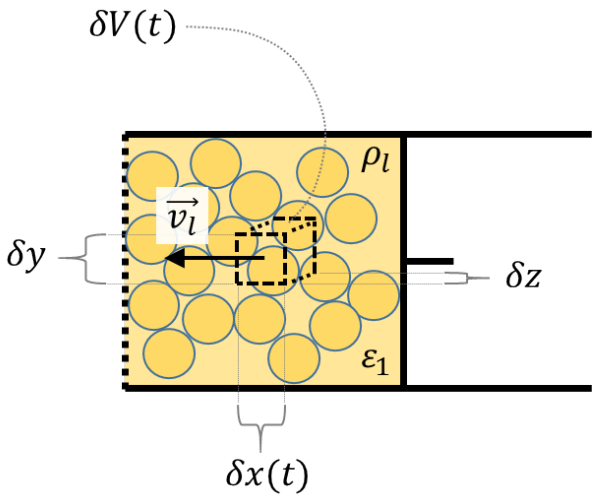

Figure 2.4: Conservation of mass for a small filter cake volume $\delta V(t) = \delta x(t) \cdot \delta y \cdot \delta z$.

Once more, integration over a tiny volume $\delta V(t)$ (depicted in figure 2.4) and application of the above mentioned theorems is performed to arrive at:

$$\frac{\mathrm{d}}{\mathrm{d}t} \int_{\delta V(t)} (\varepsilon_1 \rho_l) \mathrm{d}V + \int_{\delta V(t)} \vec{\nabla} \cdot [\varepsilon_1 \rho_l (\vec{v}_l - \vec{v}_s)] \mathrm{d}V = 0. \tag{2.13}$$

Following the same considerations as above concerning δV and geometry, assuming the oil to be incompressible yields:

$$\frac{\mathrm{d}}{\mathrm{d}t} \int_{\delta x(t)} \varepsilon_1 \mathrm{d}x + \int_{\delta x(t)} \frac{\partial[\varepsilon_1 (v_{l,x} - v_{s,x})]}{\partial x} \mathrm{d}x = 0. \tag{2.14}$$

Using the transformation of equation 2.11, letting $v_\sigma \equiv \varepsilon_1 (v_{l,x} - v_{s,x})$ denote the superficial velocity, taking the time derivative inside the integral and noting that the expression must hold for any slice, simplifies equation 2.14 to:

$$\frac{\partial}{\partial t} \frac{\varepsilon_1}{s} = -\frac{\partial v_\sigma}{\partial \omega} \tag{2.15}$$

2.3.2. CONSERVATION OF MOMENTUM

Conservation of momentum for the solid phase in 1D can be written as [29]:

$$s\rho_s \frac{\mathrm{D}^s v_{s,x}}{\mathrm{D}\,t} = -\frac{\partial \tau_{xx}}{\partial x} + F_d - s\rho_s g. \tag{2.16}$$

In this equation $\frac{\mathrm{D}^s v_{s,x}}{\mathrm{D}\,t}$ indicates the material derivative of $v_{s,x}$ moving with the solid phase [30]. $v_{s,x}$ is the x-component of $\vec{v}_s$. τ_{xx} is the principal stress in the x-direction. It is equal to the solid pressure p_s that is encountered frequently in filtration literature ($p_s \equiv \tau_{xx}$). F_d is the force per unit volume of the liquid phase on the solid phase due to the flow of the liquid, i.e. a drag force.
If the gravitational term g is negligible in comparison to the solid pressure gradient, equation 2.16 becomes:

$$0 = -\frac{\partial p_s}{\partial x} + F_d \tag{2.17}$$

In parallel, the Navier-Stokes equation for the interaggregate liquid can be stated as [29]:

$$\varepsilon_1 \rho_l \frac{\mathrm{D}\,\vec{v}}{\mathrm{D}\,t} = -\vec{\nabla} p_l - \vec{F}_d + \mu \nabla^2 \vec{v} + \varepsilon_1 \rho_l \vec{g}, \tag{2.18}$$

in which p_l is the liquid pressure, μ is the viscosity of the liquid and $\vec{g}$ is the gravitational acceleration. In pressure filtration the assumption of creeping flow i.e. $Re_h \ll 1$ is usually valid. The Reynolds number based on hydraulic diameter of the interaggregate pores, Re_h, has the aggregate diameter d_p as a characteristic length scale [31]:

$$Re_h = \frac{2}{3} \frac{\rho_l v_\sigma d_p}{s_1 \mu} \tag{2.19}$$

In the creeping flow regime the inertial terms can be neglected. Furthermore, in pressure filtration the gravitational force is small in comparison to the pressure force. Finally, because $d_p \ll L_y$ and $d_p \ll L_z$, with L_y and L_z the characteristic dimensions of the filter chambers perpendicular to the main flow, wall effects can be neglected and therefore the viscous term can be dropped, reducing equation 2.18 to:

$$0 = -\frac{\partial p_l}{\partial x} - F_d, \tag{2.20}$$

Following the suggestion of Brinkman [32], the drag force F_d is proportional to the superficial velocity of the liquid and inversely proportional to the permeability k of the filter cake:

$$F_d = \frac{\mu}{k} v_\sigma, \tag{2.21}$$

Substituting this expression in equation 2.20 gives a relation which is a modified version of Darcy's law [33]:

$$v_\sigma = -\frac{k}{\mu} \frac{\partial p_l}{\partial x}. \tag{2.22}$$

Another useful result can be obtained by addition of formulas 2.17 and 2.20:

$$\frac{\partial p_l}{\partial x} + \frac{\partial p_s}{\partial x} = 0, \tag{2.23}$$

which expresses that locally the pressure force due to the liquid pressure is in equilibrium with the stress on the filter cake at all times.
Integration of equation 2.23 shows that the sum of the liquid and solid pressure equals the pressure drop over the whole cake Δp_k:

$$p_l(x) + p_s(x) = p_s(0) = \Delta p_k \tag{2.24}$$

2.4. FLOW RESISTANCE IN A FILTER CAKE

In analogy with Ohm's law, for a porous slab of thickness $\mathrm{d}x$ with permeability $k(x)$ the local flow resistance $\mathrm{d}R$ can be defined as:

$$\mathrm{d}R \equiv \frac{\mathrm{d}x}{k(x)}. \tag{2.25}$$

Integration over the filter cake with length L gives the total flow resistance of the filter cake R_k:

$$R_k = \int_0^L \frac{1}{k(x)} \mathrm{d}x. \tag{2.26}$$

This allows for a reformulation of equation 2.22:

$$v_\sigma = \frac{\Delta p_k}{\mu R_k}. \tag{2.27}$$

2.5. LAMINAR FLOW THROUGH A SOLID SPHERE PACKING

As stated in section 2.2, a filter cake composed of aggregates resembles a mono-disperse sphere packing. For laminar flow through a mono disperse collection of spheres there exist multiple relations describing permeability as a function of porosity and particle size. In the filter cake, particle size is characterised by the aggregate diameter d_p. The Kozeny-Carman equation is often encountered in industry. It describes the strong dependence of permeability on particle size and porosity as [13]:

$$k = \frac{d_p^2}{180} \frac{\varepsilon_1^3}{(1-\varepsilon_1)^2}. \tag{2.28}$$

Generally, k and ε_1 are functions of location in the cake x.
The ordering of the spheres gives rise to different porosities. The corresponding solidosity is also known as the packing fraction. If the spheres are considered incompressible there exists a maximum close packing fraction $s_1^{hcp} = 0.74$ [34]. In practice, however, this packing fraction might not be achieved due to the random nature of the process and its lack of time. The packing is more likely to attain a random close packing fraction $s_1^{rcp} = 1 - \varepsilon_1^{rcp} \approx 0.64$ [34]. Before this fraction is reached in pressure filtration, the filter chamber average ε_1 is larger than ε_1^{rcp}, the porosity at random close packing. This stage is referred to as the *filtration step* (see figure 2.5).
Sphere configurations with porosities lower than the random close packing porosity can only be obtained by compressing the spheres. In soil mechanics this process is known as consolidation. In pressure filtration, it starts when the piston begins to touch the

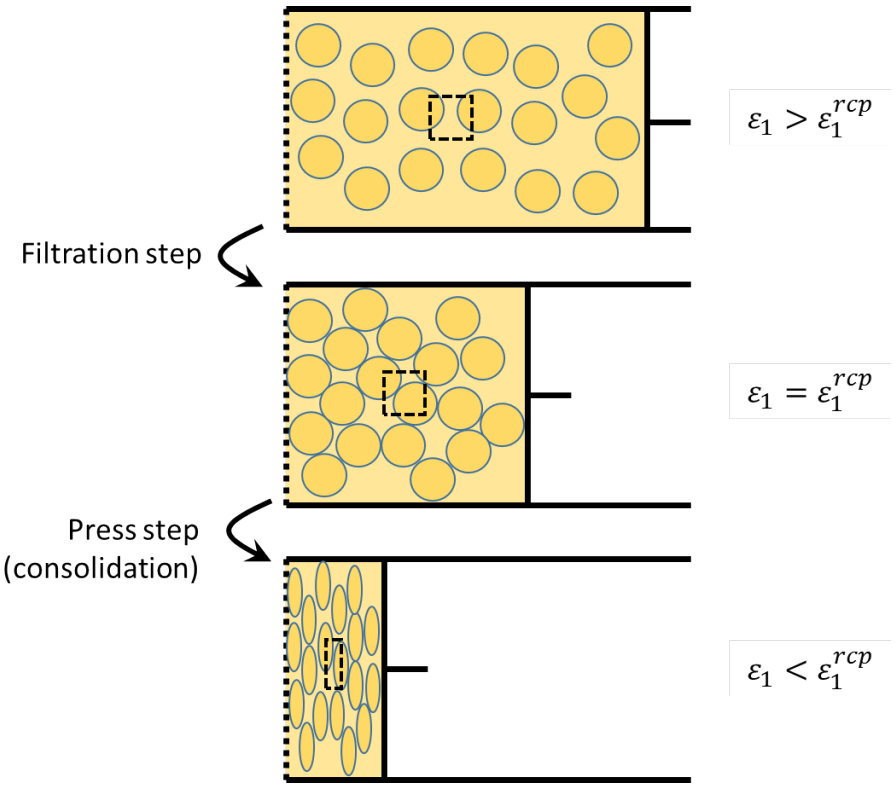

Figure 2.5: Stages in pressure filtration are discriminated through the interaggregate porosity. $\varepsilon_1 = \varepsilon_1^{rcp}$ forms the boundary between *filtration step* and *press step*.

spheres. As a stage, it is referred to here as the *press step*. It follows after the filtration step (see figure 2.5). For consolidation ($\varepsilon_1 < \varepsilon_1^{rcp}$) experiments have shown that Kozeny-Carman is no longer valid [35, 36]. A similar relation for the permeability of a porous medium in consolidation is given by Meyer and Smith [37]:

$$k = \frac{d_p^2}{90} \frac{\varepsilon_1^{4.1}}{(1-\varepsilon_1)^2}. \tag{2.29}$$

Often however, it is found that relations for k give rather big errors on the order of 50% and experimental relations for the permeability as function of porosity are used [35]. During an experiment on an AMF crystal aggregate slurry, it was found that the Meyer and Smith relation improved the permeability estimation of the Kozeny-Carman relation by half an order of magnitude [38].

2.6. LARGE DEFORMATIONS OF A POROUS MEDIUM

A measure of the relative change in length of a porous medium in compression is the strain. In our case of interest, large one-dimensional deformations are encountered and

therefore the logarithmic strain ε_{ls} is used. This thesis only deals with compression, hence a convenient sign convention leads to the following definition:

$$\varepsilon_{ls} = -\ln\left(\frac{\delta x(t)}{\delta x_u}\right), \tag{2.30}$$

where δx_u is the thickness of a porous medium slice before deformation. Using definitions 2.1, 2.2 and 2.5 introduced earlier together with conservation of mass (equation 2.10) for a deformed porous medium a relationship between strain and total void ratio can be derived:

$$\varepsilon_{ls} = -\ln\left(\frac{1+e}{1+e_0}\right). \tag{2.31}$$

Here e_0 corresponds to the total void ratio of the porous medium before deformation (i.e. at random close packing).
For a non-linear elastic semisolid an elastic modulus $E(\varepsilon_{ls})$ can be determined from the slope of the stress (p_s) versus strain curve as follows:

$$E(\varepsilon_{ls}) = \frac{\mathrm{d}p_s}{\mathrm{d}\varepsilon_{ls}}. \tag{2.32}$$

3

PRESSURE FILTRATION MODEL

In this chapter the model for pressure filtration is developed. The model is built upon results obtained in chapter 2. Apart from similarity in the formulation of the conservation equations, this model is different from the models used by Lanoisellé et al [18] and Kamst [39].
First, the conservation equations are revisited to implement the aggregates as a source term for interaggregate oil. After that, the source term is elaborated, before putting all the equations explicitly in terms of void ratios. The chapter is concluded with sections on the boundary and initial conditions that are applied in the pressure filtration model.

3.1. CONSERVATION OF INTERAGGREGATE OIL WITH SOURCES

When a crystal aggregate is compressed, its volume changes. As the intrinsic densities of the oil and fat are assumed constant, this can only be accomplished by a release of oil from the aggregate. This is modelled by treating the aggregates as sources of interaggregate oil and therefore equation 2.12 needs slight modification:

$$\frac{\partial(\varepsilon_1 \rho_l)}{\partial t} + \vec{\nabla} \cdot (\varepsilon_1 \rho_l \vec{v}_l) = s_1 \rho_l q, \tag{3.1}$$

where q is the production of interaggregate oil volume per aggregate volume (in s^{-1}). Following the same steps as in the derivation that leads to equation 2.15, a result can be obtained that is similar, apart from the source term:

$$\underbrace{\frac{\partial}{\partial t}\frac{\varepsilon_1}{s}}_{\text{Accumulation}} = \underbrace{-\frac{\partial v_\sigma}{\partial \omega}}_{\text{Diffusion}} + \underbrace{\frac{q}{s_2}}_{\text{Source}} \tag{3.2}$$

The equation shows that the problem is essentially one-dimensional. The second term in the equation might be recognised as a convective term instead. However, its diffusive character will become clear later in this section.

The accumulation term
The accumulation term can be rewritten as follows:

$$\frac{\partial}{\partial t}\frac{\varepsilon_1}{s} = (1+e_2)\frac{\partial e_1}{\partial t} + e_1\frac{\partial e_2}{\partial t} \tag{3.3}$$

The diffusion term
The diffusion term label will become clear by invoking Darcy's law (equation 2.22) in which the viscosity is taken constant over the filter chamber:

$$-\frac{\partial v_\sigma}{\partial \omega} = \frac{1}{\mu}\frac{\partial}{\partial \omega}k_1\frac{\partial p_l}{\partial x}. \tag{3.4}$$

The permeability of the interaggregate volume is denoted $k_1 = k_1(e_1)$.
Focussing on the liquid pressure gradient which plays an important role in the model, making use of equations 2.23 and 2.32 and applying the chain rule twice:

$$\frac{\partial p_l}{\partial x} \overset{(2.23)}{=} -\frac{\partial p_s}{\partial x} = -\frac{\partial p_s}{\partial \omega}\frac{\partial \omega}{\partial x} = -s\frac{\partial p_s}{\partial \omega} = -s\frac{\partial p_s}{\partial \varepsilon_{ls}}\frac{\partial \varepsilon_{ls}}{\partial e_1}\frac{\partial e_1}{\partial \omega} \overset{(2.32)}{=} \frac{sE}{1+e_1}\frac{\partial e_1}{\partial \omega}, \tag{3.5}$$

so that the pressure gradient can be seen to be linked to the gradient of the interaggregate void ratio with respect to ω:

$$\frac{\partial p_l}{\partial x} = \frac{E}{(1+e_1)^2}\frac{1}{(1+e_2)}\frac{\partial e_1}{\partial \omega}. \tag{3.6}$$

Applying this result to the diffusion term:

$$-\frac{\partial v_\sigma}{\partial \omega} = \frac{1}{\mu}\frac{\partial}{\partial \omega}\frac{k_1 E}{(1+e_1)^2}\frac{1}{(1+e_2)}\frac{\partial e_1}{\partial \omega}, \tag{3.7}$$

where the elastic modulus of the filter cake E can be determined from a constant load experiment. This modulus depends on the filter cake strain and therefore $E = E(e_1, e_2)$. The diffusion term can now be recognised as such, as it is written in terms of a second order derivative of the density like variable e_1 with respect to the spatial coordinate ω. This diffusive formulation is not uncommon, see e.g. Olivier et al.[33]

The source term
Finally, the source term can be reformulated:

$$\frac{q}{s_2} = (1+e_2)q \tag{3.8}$$

The production $q = q(e_1, e_2)$ will be explored later on.

Putting all terms together gives:

$$\underbrace{(1+e_2)\frac{\partial e_1}{\partial t} + e_1\frac{\partial e_2}{\partial t}}_{\text{Accumulation}} = \underbrace{\frac{1}{\mu}\frac{\partial}{\partial \omega}\frac{k_1 E}{(1+e_1)^2}\frac{1}{(1+e_2)}\frac{\partial e_1}{\partial \omega}}_{\text{Diffusion}} + \underbrace{(1+e_2)q}_{\text{Source}}. \tag{3.9}$$

Rearranging:

$$\frac{\partial e_1}{\partial t} = \frac{1}{(1+e_2)}\left[\frac{1}{\mu}\frac{\partial}{\partial \omega}\frac{k_1 E}{(1+e_1)^2}\frac{1}{(1+e_2)}\frac{\partial e_1}{\partial \omega} - e_1\frac{\partial e_2}{\partial t} + (1+e_2)q\right], \tag{3.10}$$

leaving a second order differential equation for the interaggregate void ratio which is coupled with the differential equation for the aggregate void ratio.

3.2. CONSERVATION OF AGGREGATE OIL

The conservation of aggregate oil is formulated in a way similar to the conservation of interaggregate oil as in equation 3.1:

$$\frac{\partial(s_1\varepsilon_2\rho_l)}{\partial t} + \vec{\nabla}\cdot(s_1\varepsilon_2\rho_l\vec{v}_{l_2}) = -s_1\rho_l q. \tag{3.11}$$

Here, $\vec{v}_{l,2}$ is the velocity of the oil within the aggregates.
Once more, the derivation follows the same steps as is done going from equation 2.12 to equation 2.15 and writing $v_{\sigma_2} = s_1\varepsilon_2(v_{l_2,x} - v_{s,x})$ as the superficial velocity of the oil within the aggregates to arrive at:

$$\frac{\partial e_2}{\partial t} + \underbrace{\frac{\partial}{\partial \omega}\left(\frac{v_{\sigma_2}}{s}\right)}_{\approx 0} = -(1+e_2)q. \tag{3.12}$$

The second term in equation 3.12 is taken to be negligible as it is assumed that oil transport mainly takes place through the interaggregate volume as it conducts the oil a lot better.

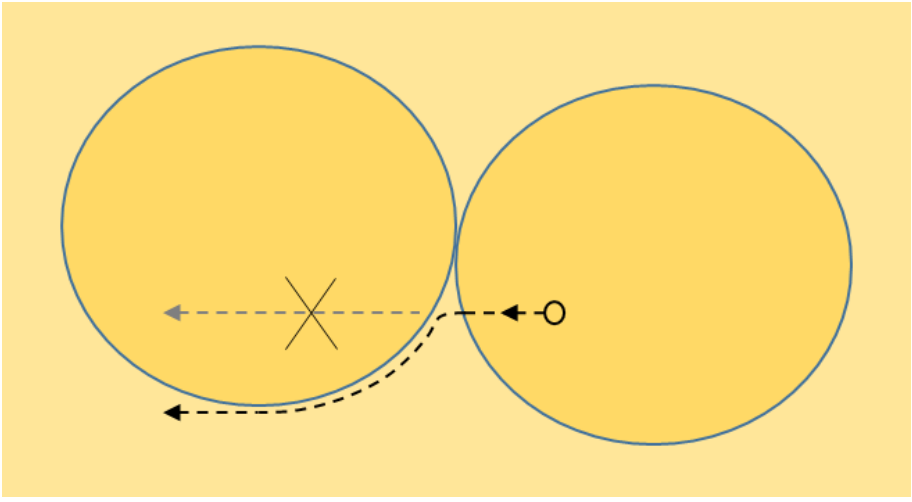

Figure 3.1: Looking through the eye of an oil parcel being squeezed out of an aggregate: Oil transport mainly takes place through the interaggregate volume as it conducts the oil a lot better.

port mainly takes place through the interaggregate volume. This idea is sketched in figure 3.1. This assumption is justified by the fact that the permeability of the interaggregate

volume is orders of magnitude larger than the permeability of the aggregates. A difference that arises due to a difference in characteristic length scales and the dependence of permeability on this characteristic length scale as can be verified with the relation of Meyer and Smith (equation 2.29). The resulting equation for the aggregate void ratio is:

$$\frac{\partial e_2}{\partial t} = -(1+e_2)q. \tag{3.13}$$

This result can be taken to rewrite the equation for the interaggregate void ratio as follows:

$$\frac{\partial e_1}{\partial t} = \frac{1}{\mu(1+e_2)}\frac{\partial}{\partial \omega}\frac{k_1 E}{(1+e_1)^2}\frac{1}{(1+e_2)}\frac{\partial e_1}{\partial \omega} + (1+e_1)q. \tag{3.14}$$

The production of interaggregate oil q, which couples both differential equations 3.13 and 3.14, will be elaborated in the next section.

3.3. PRODUCTION OF INTERAGGREGATE OIL (I)

The production of interaggregate oil arises from transport of oil from within the aggregates to the interaggregate volume due to compression of the aggregates. It can be written as the product of the aggregate area per volume a, and the flux of oil from inside the aggregate outwards, $v_{l,a\to ia}$, as follows:

$$q = a \cdot v_{l,a\to ia} = \frac{\pi d_p^2}{(\pi/6)d_p^3}\cdot\frac{k_2}{\mu}\left|-\frac{\partial p_l}{\partial x}\right| = \frac{6}{d_p}\cdot\frac{k_2}{\mu}\left|\frac{\partial p_l}{\partial x}\right|, \tag{3.15}$$

where $a = 6/d_p$ for spherulitic aggregates with diameter d_p. It is assumed that the flow out of the aggregates is Darcian, with a permeability based on the permeability of the aggregates $k_2 = k_2(e_2)$ and the characteristic length within the aggregates equal to the size of its fat crystals. Furthermore, the effective pressure gradient responsible for oil flow from inside to outside of the aggregates is taken to be the pressure gradient in which the aggregate is immersed, i.e. the pressure gradient present in the interaggregate volume. Aggregates subject to compression release oil regardless of the direction of this pressure

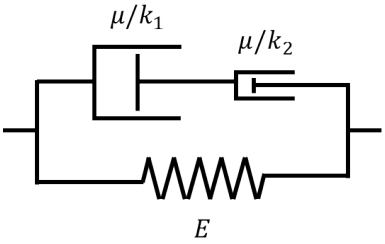

Figure 3.2: The rheological model for the milk fat filter cake: two dashpots in series in parallel with a spring.

gradient, hence the absolute value of the pressure gradient determines production. Also it is assumed that the diameter of the aggregates does not change, i.e. d_p is constant although the size of the aggregates changes as aggregate oil flows out during compression.

Moreover, the full surface of the aggregates is taken to be susceptible of oil transport to the interaggregate volume.
Equation 3.15, together with equation 2.23, completes the rheological model describing the viscoelastic behaviour of the slurry. It can be represented by two dashpots in series, in parallel with one spring as depicted in figure 3.2.

The result for the pressure gradient obtained earlier in equation 3.6, can be used to rephrase equation 3.15:

$$q = \frac{6}{d_p} \cdot \frac{k_2}{\mu} \frac{E}{(1+e_1)^2} \frac{1}{(1+e_2)} \left| \frac{\partial e_1}{\partial \omega} \right|. \tag{3.16}$$

3.4. VOID RATIO DEPENDENCE

In this section, all the equations that describe the compression of the filter cake are put in terms of the void ratios e_1 and e_2, starting with the differential equation of the interaggregate void ratio e_1.

3.4.1. THE DIFFERENTIAL EQUATION OF THE INTERAGGREGATE VOID RATIO

For reasons mentioned in section 2.5, the relation of Meyer and Smith (equation 2.29) is used for the permeability of the interaggregate volume k_1:

$$k_1 = \frac{d_p^2}{90} \frac{\varepsilon_1^{4.1}}{(1-\varepsilon_1)^2} = \frac{d_p^2}{90} \frac{e_1^{4.1}}{(1+e_1)^{2.1}}. \tag{3.17}$$

The elastic modulus can be determined from experiments by fitting an exponential function with coefficients c_1 and c_2 through measurements of strain ε_{ls} at constant load p_s in the following way:

$$p_s = c_1 \exp(c_2 \varepsilon_{ls}) - c_1. \tag{3.18}$$

Then, following definition 2.32, the elastic modulus of the filter cake can be expressed as:

$$E(\varepsilon_{ls}) = \frac{\mathrm{d}p_s}{\mathrm{d}\varepsilon_{ls}} = c_1 c_2 \exp(c_2 \varepsilon_{ls}). \tag{3.19}$$

Substituting for the strain using equation 2.31:

$$E(e_1, e_2) = c_1 c_2 \left(\frac{1+e_0}{(1+e_1)(1+e_2)} \right)^{c_2}. \tag{3.20}$$

Putting the results for the permeability and the elastic modulus into the differential equation for the interaggregate oil (equation 3.14), putting terms that are constant with respect to ω in front of the operator and contracting them with:

$$c_{e_1} = \frac{c_1 c_2 d_p^2}{90\mu} (1+e_0)^{c_2}, \tag{3.21}$$

yields:

$$\frac{\partial e_1}{\partial t} = \frac{c_{e_1}}{(1+e_2)} \frac{\partial}{\partial \omega} \left[\left(\frac{e_1}{1+e_1} \right)^{4.1} \left(\frac{1}{(1+e_1)(1+e_2)} \right)^{c_2} \frac{1}{(1+e_2)} \frac{\partial e_1}{\partial \omega} \right] + (1+e_1) q, \tag{3.22}$$

which can be rewritten in terms of the consolidation coefficient $C_e(e_1, e_2)$:

$$C_e(e_1,e_2) = c_{e_1}\left(\frac{e_1}{1+e_1}\right)^{4.1}\left(\frac{1}{(1+e_1)(1+e_2)}\right)^{c_2}\frac{1}{(1+e_2)}, \tag{3.23}$$

as:

$$\frac{\partial e_1}{\partial t} = \frac{1}{(1+e_2)}\frac{\partial}{\partial \omega}\left[C_e(e_1,e_2)\frac{\partial e_1}{\partial \omega}\right] + (1+e_1)q. \tag{3.24}$$

In this formulation, the constant c_{e_1} can be identified as a maximum for the variable consolidation coefficient $C_e(e_1, e_2)$.

3.4.2. PRODUCTION OF INTERAGGREGATE OIL (II)

In the production term, the permeability of the aggregates k_2 is once more described by the Meyer and Smith relation. In this permeability, the characteristic diameter of the crystals d_c and the porosity of the aggregates ε_2 are used:

$$k_2 = \frac{d_c^2}{90}\frac{\varepsilon_2^{4.1}}{(1-\varepsilon_2)^2} = \frac{d_c^2}{90}\frac{e_2^{4.1}}{(1+e_2)^{2.1}}. \tag{3.25}$$

Putting this expression together with relation 3.20 into equation 3.16 yields:

$$q = \frac{6}{90\mu}\frac{d_c^2}{d_p}\cdot c_1 c_2 \frac{(1+e_0)^{c_2}}{(1+e_1)^{2+c_2}}\frac{e_2^{4.1}}{(1+e_2)^{3.1+c_2}}\left|\frac{\partial e_1}{\partial \omega}\right|. \tag{3.26}$$

Contracting constants with:

$$c_q = \frac{6}{90\mu}\frac{d_c^2}{d_p}\cdot c_1 c_2 (1+e_0)^{c_2} = \frac{6d_c^2}{d_p^3}\cdot c_{e_1}, \tag{3.27}$$

results in:

$$q = \frac{c_q}{(1+e_1)^{2+c_2}}\frac{e_2^{4.1}}{(1+e_2)^{3.1+c_2}}\left|\frac{\partial e_1}{\partial \omega}\right|. \tag{3.28}$$

3.5. SUMMARY OF THE EQUATIONS

In this section, a summary of the equations that need to be solved for the press step in the pressure filtration model is presented:

Equation 3.24, describing the evolution of the interaggregate void ratio:

$$\frac{\partial e_1}{\partial t} = \frac{c_{e_1}}{(1+e_2)}\frac{\partial}{\partial \omega}\left[\left(\frac{e_1}{1+e_1}\right)^{4.1}\left(\frac{1}{(1+e_1)(1+e_2)}\right)^{c_2}\frac{1}{(1+e_2)}\frac{\partial e_1}{\partial \omega}\right] + (1+e_1)q, \tag{3.29}$$

with a maximum for the variable consolidation coefficient:

$$c_{e_1} = \frac{c_1 c_2 d_p^2}{90\mu}(1+e_0)^{c_2}. \tag{3.30}$$

Formula 3.13, describing the change with respect to time of the aggregate void ratio:

$$\frac{\partial e_2}{\partial t} = -(1+e_2)\,q. \tag{3.31}$$

And the production term q connecting both differential equations that was found in equation 3.28:

$$q = \frac{c_q}{(1+e_1)^{2+c_2}} \frac{e_2^{4.1}}{(1+e_2)^{3.1+c_2}} \left| \frac{\partial e_1}{\partial \omega} \right|, \tag{3.32}$$

with:

$$c_q = \frac{6d_c^2}{d_p^3} \cdot c_{e_1}. \tag{3.33}$$

3.6. DOMAIN AND BOUNDARY CONDITIONS

The membrane plate filter press has filter chambers which in this thesis are assumed to resemble rectangular cuboids. The chambers have filter cloths on both sides, which presents a symmetric problem. The symmetry is illustrated in figure 3.3. It follows from symmetry, that a domain with a length of $2L(t)$ with filter cloths on both sides behaves as a domain with a length of $L(t)$ with a filter cloth on only one side. The latter is chosen in this thesis to simplify analysis. Hence, the domain starts from $\omega = 0$, denoted boundary Γ_1, the position of the cloth, and runs up to $\omega = \Omega$, denoted Γ_2, the position of the piston as is indicated in figure 3.4. The cloth is assumed to be infinitely thin. Advantage is taken from using the ω-coordinate system: in ω both boundaries are static, while in x one would be dealing with a moving boundary problem, as the piston is moving. The one-dimensional character of the problem was already mentioned below equation 3.2.

The boundary condition for the piston at $\omega = \Omega$ is a no-penetration i.e. Neumann boundary condition for all modes of operation. However, the boundary condition for the cloth at $\omega = 0$ does depend on the mode of operation of the filter press.
During the filling mode, the first part is recognised as the filtration step as discussed in section 2.5. The filtration step is not modelled in this thesis. When the interaggregate porosity passes the point where it is lower than the interaggregate porosity at random close packing, i.e. $\varepsilon_1 < \varepsilon_1^{rcp}$, the press step starts as was explained in section 2.5. In experiments it was found that the press step already occurs in the filling mode [38]. In this final stage of the filling step a Dirichlet boundary condition is imposed at $\omega = 0$.
Between the filling mode and the pressing mode there can be a period of rest which is named *rest mode* here. This mode is modelled with Neumann boundary conditions on both sides of the domain.
When the pressing mode starts, the press step is continued and hence the boundary condition for the cloth side is changed back to the Dirichlet boundary condition. The various boundary conditions within the different modes of operation are summarised in table 3.1.

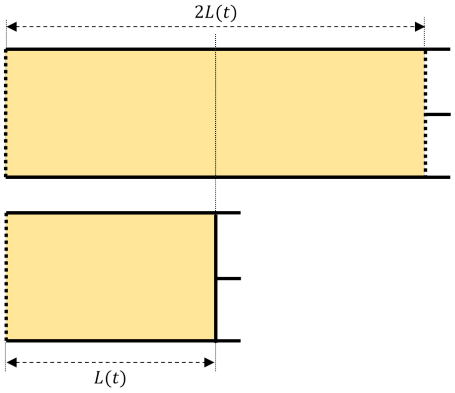

Figure 3.3: The symmetry of the filter chambers is exploited in this thesis.

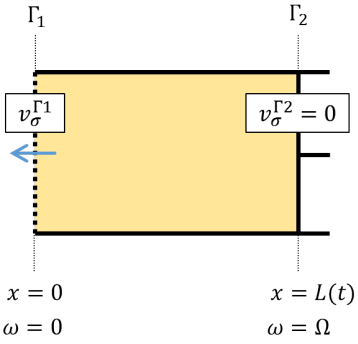

Figure 3.4: The domain which represents half a filter chamber with its boundaries.

3.6.1. DIRICHLET BOUNDARY CONDITION

The boundary condition on the cloth side during the press step is an effect of the over pressure that is being applied by the piston $p_p(t)$. In general, this applied pressure is a function of time and this function can be modified. This pressure is in equilibrium with the total pressure drop Δp_t over the domain at all times, i.e.: $p_p(t) = \Delta p_t(t)$. Due to the fact that the oil flows through the filter cake and the cloth, the liquid pressure drop takes place over both, i.e.:

$$\Delta p_t = \Delta p_k + \Delta p_d, \tag{3.34}$$

where Δp_d is the pressure drop over the cloth. Together with equation 2.27 it can be found that the pressure drop over the cake Δp_k can be calculated with:

$$\Delta p_k = \frac{p_p}{1 + R_d / R_k}. \tag{3.35}$$

In this equation R_d is the flow resistance of the cloth and R_k is the flow resistance of the filter cake which can be found by using equation 2.26.

Table 3.1: The various types of boundary conditions within the different modes of operation.

		Boundary condition	
Mode of operation	**Step**	Γ_1 ($\omega = 0$)	Γ_2 ($\omega = \Omega$)
Filling mode $(\varepsilon_1 > \varepsilon_1^{rcp})$	filtration	n/a (not modelled)	n/a (not modelled)
Filling mode $(\varepsilon_1 < \varepsilon_1^{rcp})$	press	Dirichlet	Neumann
Rest mode	n/a	Neumann	Neumann
Pressing mode	press	Dirichlet	Neumann

Next, the experimental relation 3.18 can be used to arrive at a boundary condition for the strain:

$$\varepsilon_{ls}^{\Gamma_1} = \frac{1}{c_2} \ln\left(\frac{\Delta p_k}{c_1} + 1\right), \tag{3.36}$$

which in turn can be translated into a boundary condition for the void ratio using 2.31:

$$e^{\Gamma_1} = \frac{1 + e_0}{\exp\left(\varepsilon_{ls}^{\Gamma_1}\right)} - 1. \tag{3.37}$$

Finally, as the boundary value for the aggregate void ratio can be determined from its differential equation (equation 3.31), the boundary condition for the interaggregate void ratio can be calculated with:

$$e_1^{\Gamma_1} = \frac{1 + e^{\Gamma_1}}{1 + e_2^{\Gamma_1}} - 1. \tag{3.38}$$

Note: it is assumed that in the pressing mode, the boundary value of the interaggregate void ratio is only changed and subject to the boundary condition when the applied pressure is higher than the pressure that is needed to obtain the boundary value that was reached after the rest mode. This is the *minimum pressure* for oil outflow in the pressing mode. It would be non-physical if a lower pressure would lead to an increased value of the boundary value i.e. oil flowing back into the filter chamber.
No boundary conditions are required for the aggregate void ratio. Both $e_2^{\Gamma_1}$ and $e_2^{\Gamma_2}$ can be obtained by solving equation 3.31, which only requires an initial condition.

3.6.2. NEUMANN BOUNDARY CONDITION

The no-penetration condition which is in place at the piston at $\omega = \Omega$ at all times and at the cloth at $\omega = 0$ during the rest mode can be summarised as:

$$[v_\sigma]^{\Gamma_1}_{\text{Rest mode}} = 0, \quad [v_\sigma]^{\Gamma_2}. \tag{3.39}$$

Equation 2.22 shows that this results in a boundary condition for the liquid pressure gradient:

$$\left[\frac{\partial p_l}{\partial x}\right]^{\Gamma_1}_{\text{Rest mode}} = 0, \quad \left[\frac{\partial p_l}{\partial x}\right]^{\Gamma_2} = 0, \tag{3.40}$$

which in turn, following equation 3.6, has a boundary condition for the interaggregate void ratio gradient with respect to ω as a consequence:

$$\left[\frac{\partial e_1}{\partial \omega}\right]^{\Gamma_1}_{\text{Rest mode}} = 0, \qquad \left[\frac{\partial e_1}{\partial \omega}\right]^{\Gamma_2} = 0. \tag{3.41}$$

3.7. INITIAL CONDITIONS

The initial condition for the interaggregate void ratio across the domain is determined by its value at random close packing:

$$e_1(\omega, 0) = \frac{\varepsilon_1^{rcp}}{s_1^{rcp}}. \tag{3.42}$$

The initial value of the aggregate void ratio over the entire domain is also calculated from known values associated with random close packing:

$$e_2(\omega, 0) = \frac{s_1^{rcp}}{s^{rcp}} - 1. \tag{3.43}$$

The solid fat volume fraction at random close packing is denoted s^{rcp}. By definition it is connected to the total void ratio of the porous medium before deformation e_0 as follows:

$$e_0 = \frac{1 - s^{rcp}}{s^{rcp}}. \tag{3.44}$$

4

NUMERICAL IMPLEMENTATION

In this chapter, a numerical implementation of the pressure filtration model is formulated. Discretisations of the domain, time, the equations and the boundary conditions are given. An estimation procedure for the ghost node concludes this chapter.

4.1. DISCRETISATION OF THE DOMAIN

The domain, which represents half a filter chamber, is discretised in a straightforward manner using a uniform grid. The interval $[0,\Omega]$ is divided into $J+1$ nodes with position $\omega^j = j\cdot\Delta\omega$. The j in superscript denotes grid position. At each side, with indices $j=1$ and $j=J+3$, a ghost node is added outside the domain, to allow for imposing boundary conditions. The discretisation of the domain is depicted in figure 4.1.
To facilitate calculating the thickness of the filter cake at any time or any other thickness averaged quantities, every interior node is assigned a length $\Delta\omega$ which has an interval $\left[\omega^j-\frac{1}{2}\Delta\omega,\omega^j+\frac{1}{2}\right]$. Both boundary nodes have half the length of an interior node i.e. $\frac{1}{2}\Delta\omega$.

4.2. DISCRETISATION OF TIME

The time step of a variable is indicated with an i in superscript. The choice for the size of the time step $\Delta t = t^{i+1}-t^i$ is connected to the choice for the magnitude of $\Delta\omega$. To impose stability in an explicit scheme, the following criterion is used:

$$Fo_\Delta = \frac{C_{e0}\cdot\Delta t}{\Delta\omega^2} < \frac{1}{2}. \tag{4.1}$$

In this relation, Fo_Δ is the local Fourier number and C_{e0} is a constant which is an overestimation of the maximum for the consolidation coefficient c_{e_1}, i.e.:

$$C_{e0} \gg c_{e_1}. \tag{4.2}$$

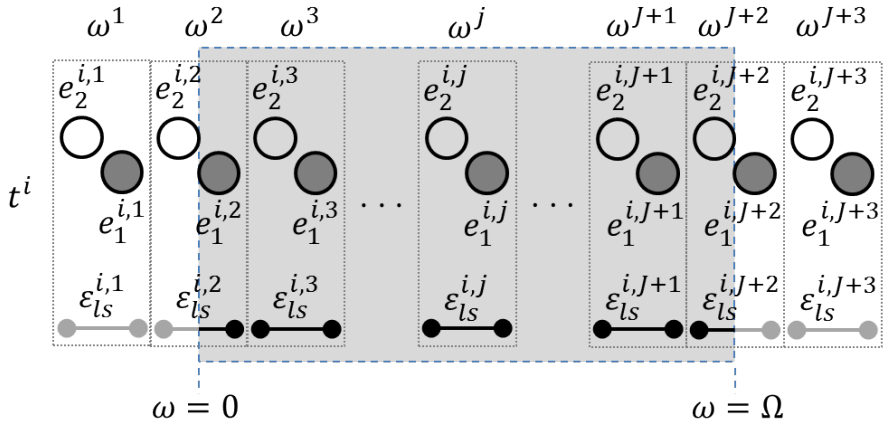

Figure 4.1: The discretisation of the domain: the shaded area represents the continuous domain with interval $[0,\Omega]$. The nodes, which are the discrete values of the void ratios are depicted as circles and the discrete strains drawn as two dots connected by a line.

4.3. DISCRETISATION OF THE EQUATIONS

The equations are solved with an Euler-forward finite-difference scheme. Recalling the differential equations of section 3.5, equations 3.29 and 3.31:

$$\frac{\partial e_1}{\partial t} = \frac{c_{e_1}}{(1+e_2)}\frac{\partial}{\partial \omega}\left[\left(\frac{e_1}{1+e_1}\right)^{4.1}\left(\frac{1}{(1+e_1)(1+e_2)}\right)^{c_2}\frac{1}{(1+e_2)}\frac{\partial e_1}{\partial \omega}\right] + (1+e_1)q, \tag{4.3}$$

which can be rewritten in a more compact form:

$$\frac{\partial e_1}{\partial t} = c_{e_1} f(e_2)\frac{\partial}{\partial \omega} g(e_1,e_2)\frac{\partial e_1}{\partial \omega} + (1+e_1)q, \tag{4.4}$$

and

$$\frac{\partial e_2}{\partial t} = -(1+e_2)q. \tag{4.5}$$

First, applying the Euler-forward scheme to the left hand side of equation 4.4:

$$\frac{\partial e_1}{\partial t} \approx \frac{e_1^{i+1,j} - e_1^{i,j}}{\Delta t}. \tag{4.6}$$

Applying the product rule to the first term on the right hand side in equation 4.4:

$$c_{e_1} f(e_2)\frac{\partial}{\partial \omega} g(e_1,e_2)\frac{\partial e_1}{\partial \omega} = c_{e_1} f(e_2)\left[g(e_1,e_2)\frac{\partial^2 e_1}{\partial \omega^2} + \frac{\partial g(e_1,e_2)}{\partial \omega}\cdot\frac{\partial e_1}{\partial \omega}\right]. \tag{4.7}$$

Using central differencing, this term can be discretised as follows:

$$c_{e_1} f^{i,j}\left[g^{i,j}\frac{e_1^{i,j+1} - 2e_1^{i,j} + e_1^{i,j-1}}{\Delta\omega^2} + \frac{g^{i,j+1} - g^{i,j-1}}{2\Delta\omega}\cdot\frac{e_1^{i,j+1} - e_1^{i,j-1}}{2\Delta\omega}\right]. \tag{4.8}$$

The second term on the right hand side in equation 4.4 can be made discrete as follows:

$$(1+e_1)q \approx \left(1+e_1^{i,j}\right) q^{i,j}. \tag{4.9}$$

The discrete result for equation 4.5 is obtained analogously:

$$\frac{e_2^{i+1,j}-e_2^{i,j}}{\Delta t} = -\left(1+e_2^{i,j}\right) q^{i,j}. \tag{4.10}$$

Focussing on the production term which was formulated in equation 3.32:

$$q = \frac{c_q}{(1+e_1)^{2+c_2}} \frac{e_2^{4.1}}{(1+e_2)^{3.1+c_2}} \left|\frac{\partial e_1}{\partial \omega}\right|. \tag{4.11}$$

It is numerically implemented with:

$$q^{i,j} = \frac{c_q}{2\Delta\omega\left(1+e_1^{i,j}\right)^{2+c_2}} \frac{\left[e_2^{i,j}\right]^{4.1}}{\left(1+e_2^{i,j}\right)^{3.1+c_2}} \cdot \text{abs}\left(e_1^{i,j+1}-e_1^{i,j-1}\right). \tag{4.12}$$

To summarise and write out the result in explicit form, the equations that determine a next time step for the void ratios are:

$$e_1^{i+1,j} = e_1^{i,j} + \Delta t \cdot \left\{ \frac{c_{e_1} f^{i,j}}{4\Delta\omega^2} \left[4g^{i,j}\left(e_1^{i,j+1} - 2e_1^{i,j} + e_1^{i,j-1}\right) + \left(g^{i,j+1}-g^{i,j-1}\right)\cdot\left(e_1^{i,j+1}-e_1^{i,j-1}\right)\right] + \left(1+e_1^{i,j}\right) q^{i,j} \right\}, \tag{4.13}$$

and

$$e_2^{i+1,j} = e_2^{i,j} - \Delta t \cdot \left(1+e_2^{i,j}\right) q^{i,j}, \tag{4.14}$$

with

$$f^{i,j} = \frac{1}{1+e_2^{i,j}}, \tag{4.15}$$

$$g^{i,j} = \left(\frac{e_1^{i,j}}{1+e_1^{i,j}}\right)^{4.1} \left(\frac{1}{\left(1+e_1^{i,j}\right)\left(1+e_2^{i,j}\right)}\right)^{c_2} f^{i,j}, \tag{4.16}$$

and the production term presented in equation 4.12:

$$q^{i,j} = \frac{c_q}{2\Delta\omega\left(1+e_1^{i,j}\right)^{2+c_2}} \frac{\left[e_2^{i,j}\right]^{4.1}}{\left(1+e_2^{i,j}\right)^{3.1+c_2}} \cdot \text{abs}\left(e_1^{i,j+1}-e_1^{i,j-1}\right). \tag{4.17}$$

4.4. DISCRETISATION OF THE BOUNDARY CONDITIONS

The discretised equations for the boundary conditions follow naturally from the equations in section 3.6. They are treated here according to type: first, the Dirichlet boundary condition and then the Neumann boundary condition.

4.4.1. DIRICHLET BOUNDARY CONDITION

A Dirichlet boundary condition is in place at boundary Γ_1 during the press step (see figure 4.1). The boundary Γ_1 corresponds to variables with index $j = 2$. The applied pressure by the piston at every time step p_p^i needs to be translated to a boundary value $e_1^{i,2}$. This is done according to the discrete counterparts of equations 3.35 to 3.38:

$$\Delta p_k^i = \frac{p_p^i}{1 + R_d / R_k^i} \quad \rightarrow \quad \varepsilon_{ls}^{i,2} = \frac{1}{c_2} \ln\left(\frac{\Delta p_k^i}{c_1} + 1\right) \quad \rightarrow \tag{4.18}$$

$$e^{i,2} = \frac{1 + e_0}{\exp\left(\varepsilon_{ls}^{i,2}\right)} - 1 \quad \rightarrow \quad e_1^{i,2} = \frac{1 + e^{i,2}}{1 + e_2^{i,2}} - 1. \tag{4.19}$$

The last equality in equation 4.19 shows that $e_2^{i,2}$ is needed to calculate $e_1^{i,2}$. From equations 4.14 and 4.17 it can be deduced that for $e_2^{i,2}$ one would need $e_1^{i-1,1}$. The latter is the value of the interaggregate void ratio with index $j = 1$ i.e. the ghost node. A scheme for estimating this value is given in section 4.5.
Finally, to calculate R_k^i in equation 4.18, equations 2.4, 2.6, 2.11, 2.26 and 2.29 can be combined to arrive at:

$$R_k^i = \frac{90\Delta\omega}{d_p^2} \cdot \sum_{j=2}^{J+2} w_R^j \frac{\left(1 + e_2^{i,j}\right)\left(1 + e_1^{i,j}\right)^{3.1}}{\left[e_1^{i,j}\right]^{4.1}}, \tag{4.20}$$

with a weighting factor w_R^j, as only half of the lengths of the boundary nodes fall within the domain:

$$w_R^j = \begin{cases} \frac{1}{2} & \text{if } j = 2 \text{ or } j = J+2 \\ 1 & \text{otherwise} \end{cases} \tag{4.21}$$

4.4.2. NEUMANN BOUNDARY CONDITION

The discrete form of the Neumann boundary condition follows from applying a central differencing scheme to equation 3.41. It is used at the node corresponding to the piston boundary at $\omega = \Omega$ with index $j = J+1$ at all times (see figure 4.1):

$$e_1^{i,J+3} = e_1^{i,J+1}. \tag{4.22}$$

The no-penetration condition is used at the node corresponding to the cloth boundary at $\omega = 0$ with index $j = 2$ during the rest mode only:

$$e_1^{i,1} = e_1^{i,3} \quad \text{(Rest mode)}. \tag{4.23}$$

4.5. A SCHEME FOR ESTIMATING THE GHOST NODE

The estimation of the ghost node is embedded in a routine. This routine will first be clarified with the help of stencils.

4.5.1. STENCILS USED FOR COMPUTATION

Stencils are given in figures 4.2-4.6, representing the numerical routine that is associated with boundary Γ_1 at ω^2.

In figure 4.2, the node points are shown, along with the associated strains that are

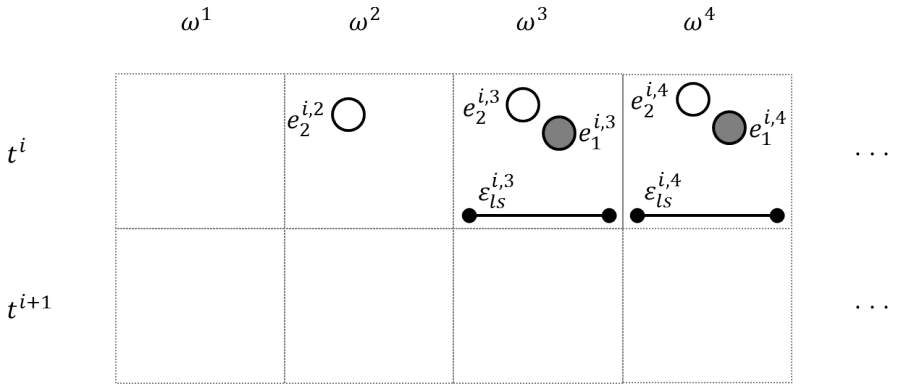

Figure 4.2: The node points together with the associated strains that are known at an arbitrary time step t^i.

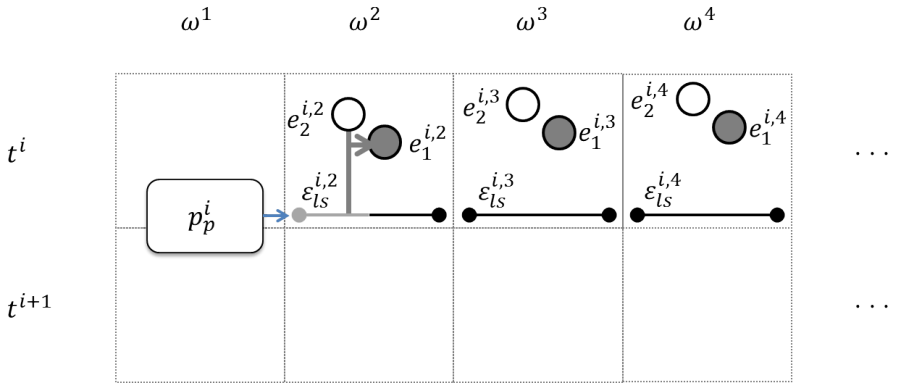

Figure 4.3: The applied pressure p_p^i ultimately determines the node $e_1^{i,2}$, locally and instantaneously squeezing out oil.

known at an arbitrary time step t^i. Moving to figure 4.3, the applied pressure p_p^i determines the strain $\varepsilon_{ls}^{i,2}$ through equation 4.18. Subsequently, the node $e_1^{i,2}$ is calculated with 4.19 using $e_2^{i,2}$ and $\varepsilon_{ls}^{i,2}$. In the next step in figure 4.4, the ghost node $e_1^{i,1}$ is extrapolated from the node points $e_1^{i,2}$, $e_1^{i,3}$ and $e_1^{i,4}$ using equation 4.24. The method for

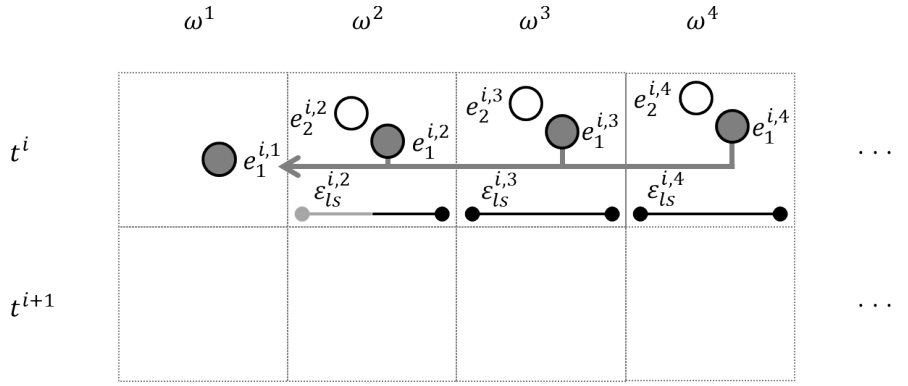

Figure 4.4: The ghost node $e_1^{i,1}$ is extrapolated from its three interaggregate neighbours.

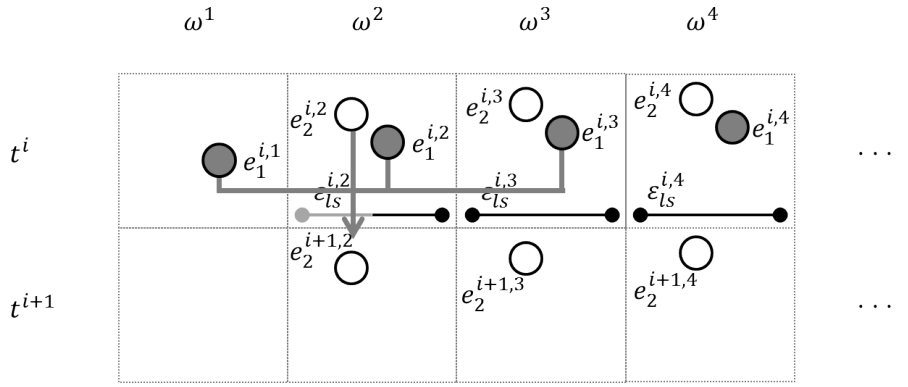

Figure 4.5: Step-wise time evolution producing $e_2^{i+1,j}$. Here the stencil is given for $e_2^{i+1,2}$ serving as a blueprint for $e_2^{i+1,j}$.

estimation is explained in subsection 4.5.2. The following image in figure 4.5 shows how the aggregate void ratio nodes of the next time step, $e_2^{i+1,j}$, are related to the void ratio nodes of the current time step $e_2^{i,j}$, $e_1^{i,j-1}$, $e_1^{i,j}$ and $e_1^{i,j+1}$, exploiting the ghost node. It is done according to equation 4.14. Continuing the algorithm with figure 4.6, where the interaggregate void ratio nodes for the new time step $e_1^{i+1,j}$ are obtained from both aggregate and interaggregate void ratio nodes from the previous time step $\left(e_1^{i,j-1}, e_1^{i,j}, e_1^{i,j+1}, e_2^{i,j-1}, e_2^{i,j}\right.$ and $\left.e_2^{i,j+1}\right)$. This is done with equation 4.13. Finally, in figure 4.7, it is made clear that this operation finalises the routine: the time step t^{i+1} contains the same amount of information that was started with in time step t^i in the first image of the series, figure 4.2.

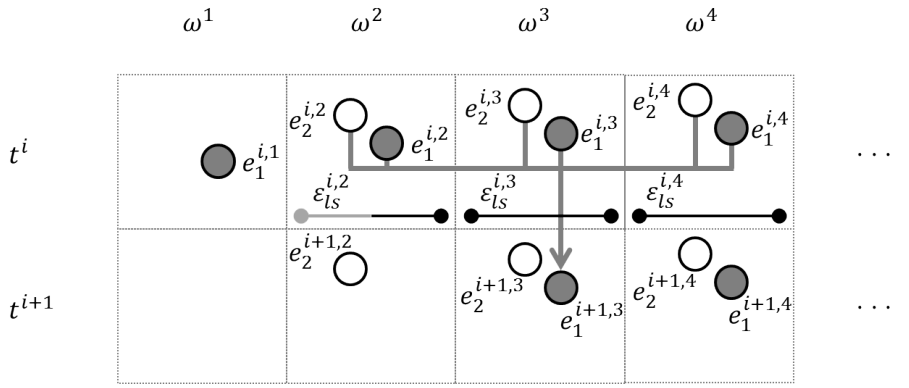

Figure 4.6: All nearby nodes from the current time step are needed to calculate the interaggregate void ratio node of the next time step $e_1^{i+1,j}$. Here the stencil is given for $e_1^{i+1,3}$, the archetype for $e_1^{i+1,j}$.

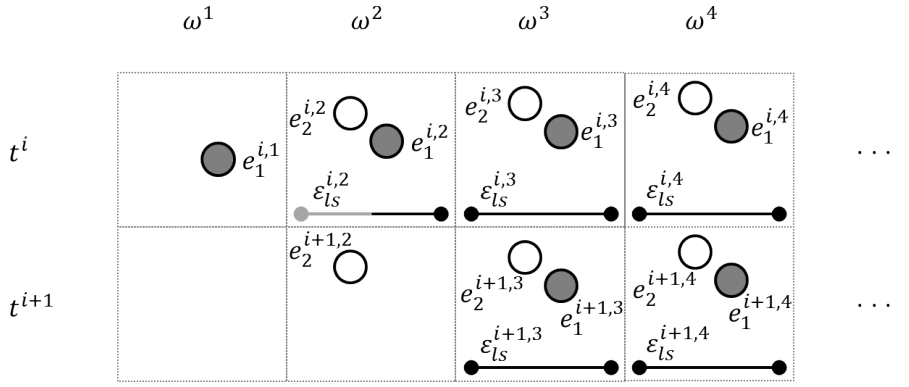

Figure 4.7: The information status for time step t^{i+1} resembles that of t^i in figure 4.2: the routine can start over again.

4.5.2. ESTIMATION OF THE GHOST NODE

Solutions for the interaggregate void ratio tend to have a square root shape. Therefore, to estimate the ghost node $e_1^{i,1}$ it is imposed that the following relation holds for the differences between interaggregate void ratio nodes depicted in figure 4.8:

$$\frac{\Delta e_1^{i,1}}{\Delta e_1^{i,2}} = \frac{\Delta e_1^{i,2}}{\Delta e_1^{i,3}}, \tag{4.24}$$

where $\Delta e_1^{i,j} = e_1^{i,j+1} - e_1^{i,j}$. However, this gives non-physical (negative) values for the ghost node when $\Delta e_1^{i,2} \gg \Delta e_1^{i,3}$ or when $\Delta e_1^{i,3} = 0$. Therefore, in case $\Delta e_1^{i,1} > 0.01$ the following is imposed:

$$\Delta e_1^{i,1} = \Delta e_1^{i,2}. \tag{4.25}$$

And when $\Delta e_1^{i,3} = 0$ it is enforced that $\Delta e_1^{i,1} = 0$.
From these considerations, it follows that the ghost node can be calculated with:

$$e_1^{i,1} = \begin{cases} e_1^{i,2} & \text{if } e_1^{i,3} = e_1^{i,4} \\ e_1^{i,2} - \frac{\left[\Delta e_1^{i,2}\right]^2}{\Delta e_1^{i,3}} & \text{if } e_1^{i,2} - \frac{\left[\Delta e_1^{i,2}\right]^2}{\Delta e_1^{i,3}} < 0.01 \\ 2e_1^{i,2} - e_1^{i,3} & \text{if } e_1^{i,2} - \frac{\left[\Delta e_1^{i,2}\right]^2}{\Delta e_1^{i,3}} > 0.01 \end{cases} \tag{4.26}$$

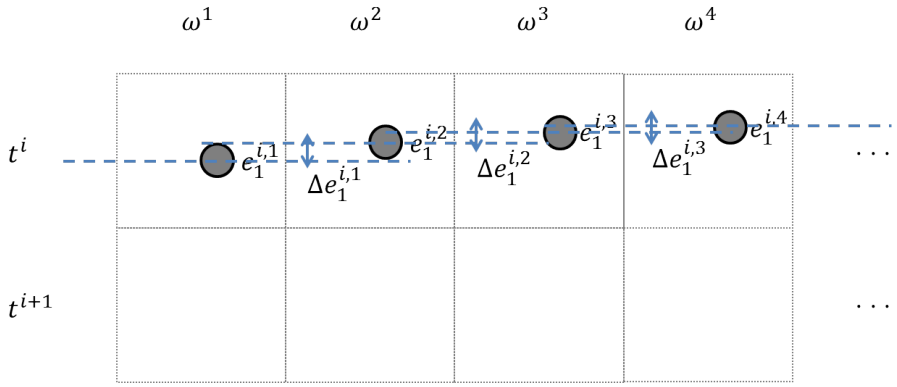

Figure 4.8: Equal ratios of differences between nodes are proposed as the solution tends to be square root shaped.

5

RESULTS

In this chapter the results of the simulations with the pressure filtration model are presented. First, simulations that were performed with the model are compared to measurements that were obtained during experiments. Thereafter, rates of pressure increase are contrasted and finally, the influence of multistep pressure profiles is studied.

5.1. COMPARISON OF SIMULATIONS WITH EXPERIMENTS

The model was numerically implemented with MATLAB R2014b to perform simulations. Before the pressure filtration model can make valuable predictions however, it has to be contrasted with measurements. These measurements have been taken from experiments conducted in a pilot plant with a small membrane filter press. Filtration experiments were done with slurries of milk fat crystal aggregates prepared on-site. More details on the experiments conducted can be found in subsection 5.1.1.
A strict comparison is challenging, as the pressure filtration model only models an idealised filter chamber. Other components of the membrane filter press are not part of the model. One can think of the tubes and pipes were slurry or oil can reside that cannot be taken into account in measurements (directly). Also assumptions have to be made regarding the filling mode. It is assumed that during the filling mode, prior to the press step, the filter cake is formed homogeneously. The pressure-time profiles used in the simulations are idealised versions of the versions applied in experiments.
Nonetheless, comparison is done as follows: first, the numerous coefficients that the model contains are estimated and calculated. Five coefficients are left to be determined by calibration (subsection 5.1.2). Then, with all coefficients fixed, graphs showing volume fractions as a function of filter chamber location are produced for a typical case in subsection 5.1.3. This is possible, as the model is capable of resolving volume fractions locally as function of time. Thereafter, pressure-time profiles are varied to study whether the model produces valid results. Validation will be done with respect to outflow velocity, eventual *SFC* and eventual *SFC* of filter cake layers in subsection 5.1.4.

5.1.1. EXPERIMENTS

The experiments were performed with a membrane filter press that is small in comparison to industrial standards. It contained five filter plates with dimensions 40 cm × 40 cm, creating 3 cm thick filter chambers. The milk fat crystal aggregate slurry was prepared from melted AMF in a crystallizer on-site. The slurry was then pumped by a slurry pump from the crystallizer into the filter chambers in the membrane filter press. The produced olein was collected in a milk churn standing on a balance to allow for calculations of the oil outflow (see figure 5.1). The weight of the olein was registered by a computer every second. Typically 20 kg of olein was produced per experiment. To convert to volume, the density of olein was taken to be 910 kg/m^3.

In total, seven successful experiments were done which are listed in table 5.1. Every

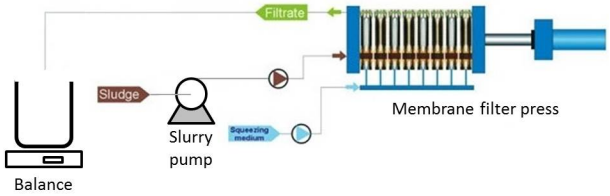

Figure 5.1: The experimental set-up used in the pilot plant: a slurry pump to transport the slurry from crystallizer to filter chambers and a milk churn on a balance to facilitate oil outflow measurements.

Table 5.1: The labels referring to seven experiments with six different pressure-time profiles. For the two pressure-time profiles used for the calibration, kal1 and kal2, the maximum rate of pressure increase (RPI) is given.

Label	**Maximum RPI (bar/min)**	**Number of steps**	**Pressing mode duration (min)**	**Date of experiment** [40]
kal1	1 (see fig. 5.2)	1	10.5	8 Nov 2017
kal2	0.5	1	15.2	14 Nov 2017
ptp1a	n/a	3	13.5	4 Oct 2017
ptp1b	n/a	3	11.8	10 Oct 2017
ptp2	n/a	4	14.9	17 Oct 2017
ptp3	n/a	3	12.7	31 Oct 2017
ptp4	n/a	3	28.1	21 Nov 2017

pressure-time profile that was applied was controlled manually. The labels in the table refer, in this thesis, to the idealised pressure-time profiles, not to the exact pressure-time profiles that were applied in the experiments. The eventual *SFC* (the *SFC* of the S fraction) was measured with a nuclear magnetic resonance (NMR) analyser.

The experiments are formally not part of this thesis. Further details regarding the experiments have been reported in earlier work [41].

5.1.2. CALIBRATION OF THE MODEL

Five coefficients of the model were taken to perform a calibration: they were varied to let the model fit the outflow velocity measured in experiments. The best fit determined the value of these coefficients.

Table 5.2: Values of model constants used in the simulations.

Quantity	Value	Units	Derivation
c_1	$3.31 \cdot 10^{-2}$	Pa	-
c_2	5.18	-	-
C_{e0}	10^{-5}	m^2/s	-
d_c	2	µm	-
L_0	2.05	cm	-
J	23	-	-
μ	0.06	Pa·s	-
$\Delta\omega$	$2.03 \cdot 10^{-4}$	m	Ω/J
Ω	0.467	cm	$s^{rcp} \cdot L_0$
R_d	$1.6 \cdot 10^9$	m^{-1}	-
s^{rcp}	0.228 [42]	-	-
Δt	$2.10 \cdot 10^{-3}$	s	$\Delta\omega^2/2C_{e0}$

The values listed in table 5.2 were used for the constants within the model. The values for c_1 and c_2 from equation 3.18 were retrieved from a least squares regression. C_{e0} was chosen based on an overestimation of c_{e_1} from equation 3.30. The effective crystal diameter d_c was estimated during a discussion with the supervisors. L_0 is the initial equivalent thickness of the filter cake if consolidation was reached purely by use of the compression chambers instead of consolidation through filling. It was obtained by calculating $\Omega/s_{0,P}$, where $s_{0,P}$ is a provisional back calculated value of the solid fat volume fraction at the start of the pressing mode (the provisional value was used to obtain a value for L_0, the value of $s_{0,P}$ was later adjusted in the calibration). J was obtained after a sensitivity analysis and chosen large enough to keep the computational burden bearable and small enough to adequately reduce errors. μ is an estimate based on the typical viscosity of oils. R_d and s^{rcp} were obtained in experiments, the first by filtering oil without solid fat [42]. s^{rcp} was obtained by measuring *SFCs* of a deposited filter cakes in centrifugation experiments. The other constants in table 5.2 are derived quantities. Density

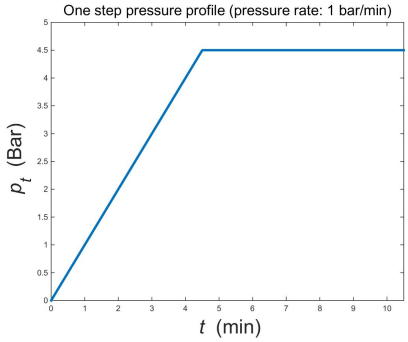

Figure 5.2: Pressure-time profile kal1: a one-step pressure-time profile: linearly increasing with a certain pressure rate followed by a constant pressure.

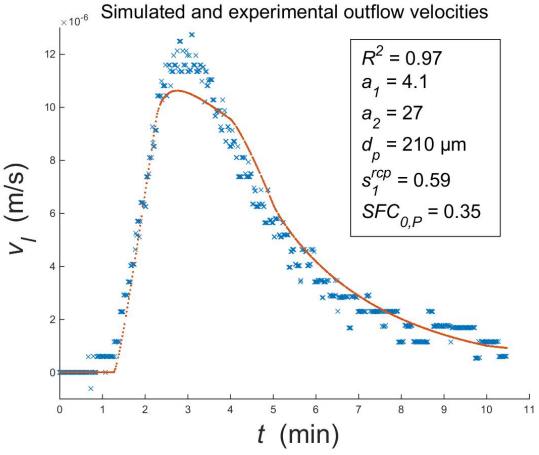

Figure 5.3: The best fit for the outflow velocity after application of pressure-time profile kal1.

differences between the solid fat and the oil were assumed negligible such that solid fat content is equal to solid fat volume:

$$SFC(\omega, t) \approx s(\omega, t) \tag{5.1}$$

With the values of 5.2, a calibration can be done by comparing a temporally resolved outflow velocity from simulation, with an outflow velocity obtained from experiment. The simulated outflow velocity v_l^i is derived from the spatially and temporally resolved filter cake thickness L^i as follows:

$$v_l^i = \frac{L^{i-1} - L^i}{\Delta t}. \tag{5.2}$$

At any time, filter cake thickness can be calculated with the following formula:

$$L^i = \Delta\omega \cdot \sum_{j=2}^{J+2} w_R^j \left(1 + e_1^{i,j}\right)\left(1 + e_2^{i,j}\right), \tag{5.3}$$

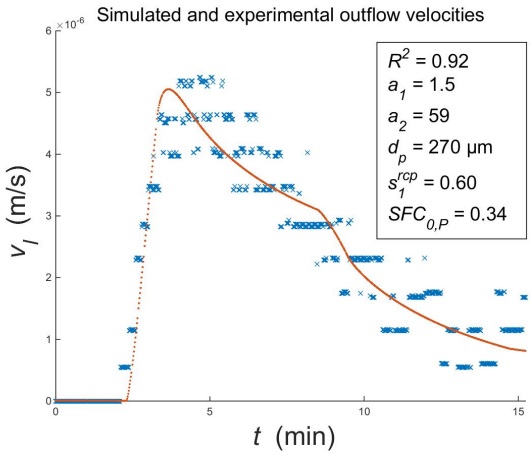

Figure 5.4: The best fit for the outflow velocity after application of pressure-time profile kal2.

where w_R^j is given by equation 4.21. Moving averages, with a period of 1 min, were obtained from both the experimental and the simulated outflow velocities before calculating a coefficient of determination (R^2) for the fit of the model.

The following five coefficients were chosen to perform a calibration:

- a_1, a flow resistance factor for the interaggregate volume
- a_2, a flow resistance factor for the aggregate volume
- d_p, the aggregate diameter
- s_1^{rcp}, the random close packing of the aggregates
- $SFC_{0,P}$, the solid fat content at the start of the pressing mode

The coefficients were varied within the boundaries that are considered physically plausible.
The flow resistance factor a_1 was added to equation 4.13 by replacing c_{e_1} by c_{e_1}/a_1. Analogously, the flow resistance factor a_2 was added to equation 4.17 by substituting c_q by c_q/a_2. The solid fat content at the start of the pressing mode was varied by varying the effective pressure responsible for expression during the filling mode. This was done by varying k_p, a multiplication factor for the pressure profile during filling. This pressure profile resembles one that was measured at the slurry pump (see figure 5.1).
Both calibrations were done with a one-step pressure-time profile (OSPP) as depicted in figure 5.2. An $R^2 = 0.97$ was obtained with pressure-time profile kal1 (figure 5.3), while an $R^2 = 0.92$ was produced with pressure-time profile kal2 (figure 5.4). The calibrations led to two different sets of coefficients which were averaged to retrieve the following set:

$$a_1 = 2.7 \quad a_2 = 42 \quad d_p = 230\ \mu\text{m} \quad s_1^{rcp} = 0.59 \quad SFC_{0,P} = 0.35 \tag{5.4}$$

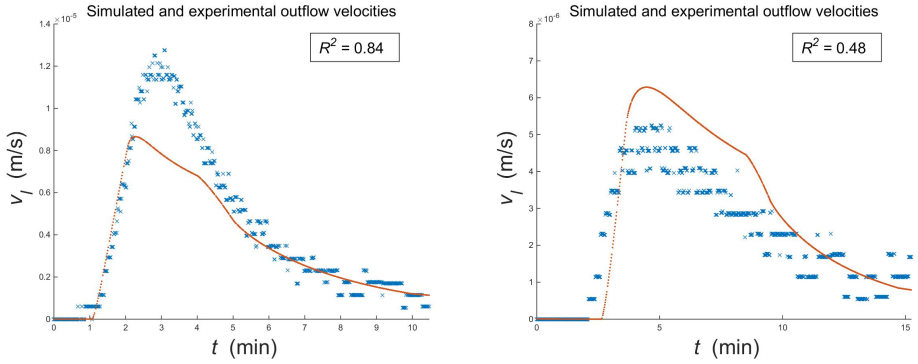

(a) *kal1* (b) *kal2*

Figure 5.5: The fit of the outflow velocity for the pressure-time profiles kal1 and kal2 using the coefficients obtained in the calibration (equation 5.4).

5

The flow resistance factor $a_1 = 2.7$ can be expected from a measurement that found Meyer & Smith's relation to overestimate the permeability by half an order of magnitude [38]. The other flow resistance factor is large with a value of 42. This can stem from the effective diameter of the crystals being an order of magnitude smaller. The aggregate diameter is on the large side with 230 µm. However, this might be ascribable to the agglomeration of aggregates, which was observed during experiments (see figure 1.3). The packing fraction $s_1^{rcp} = 0.59$ is the least dense packing associated with random close packing found in literature[34]. The solid fat content of $SFC_{0,P} = 0.35$ ($k_p = 0.85$) is 3% higher than provisional back calculated values found during experiments[38]. This might be due to oil already flown out of the cake still occupying tubes and pipes of the filter press which is not accounted for in the provisional back calculation.
In figure 5.5, the effect of the coefficients given in equation 5.4 is shown for the pressure profiles which were used in the calibration. Comparing 5.3 with 5.5a, both displaying outflow velocities for the 1 bar/min OSPP (kal1), it can be observed that the fit is still good, except for the values around the maximum which are underestimated by the model. This is a result of taking an average to determine the calibration coefficients of equation 5.4, causing a_1 to be too low and both a_2 and d_p to be too high for this pressure profile. This can be explained as follows: When taking the coefficients acquired from the 0.5 bar/min OSPP (kal2) and using them on the 1 bar/min OSPP (kal1), it seems from these experimental results that the model lacks some sensitivity with respect to rate of pressure increase (RPI), giving an underestimate for the outflow velocity. The coefficients of equation 5.4 give a better fit, but still give an underestimate.
The statement about sensitivity with respect to RPI cannot be made in general, since it is based only on two experiments.
For pressure-time profile kal2 one can see that the model picks up the outflow velocity too late in figure 5.5b. This is mainly due to the value of k_p that is relatively high. The previous fit in figure 5.4 for the first part of the outflow velocity graph was better. This is also the case for the period around the maximum between 4 and 10 minutes. With the calibration coefficients of equation 5.4 the outflow velocity is overestimated for

pressure-time profile kal2, again a result of taking an average to determine the calibration coefficients of equation 5.4, causing a_1 to be too high and both a_2 and d_p to be too low for this case.

During the calibration, it was confirmed that medium resistance is negligible compared to filter cake resistance [43]. Filter cake resistance at the beginning of the pressing mode was a factor of 20 larger than the resistance of the cloth and this factor grew to a factor of 100 during expression.

5.1.3. VOLUME FRACTIONS AS FUNCTION OF FILTER CHAMBER LOCATION

The pressure filtration model is capable of resolving volume fractions locally as function of time. During simulations the void ratios e_1 and e_2 have been solved numerically for $J-1=22$ points within the filter chamber and for every time step with $\Delta t = 2.10$ ms (table 5.2). The void ratios can be translated with equations 2.1-2.4 and 2.6 to the volume fractions ε_1, $s_1 \cdot \varepsilon_2$ and $s_1 \cdot s_2$. In this order, from the bottom upwards, these volume fractions are shown as surfaces in figure 5.6. The surfaces are plotted as function of filter chamber location measured from the cloth (indicated by the dashed line) for various operation modes and time steps. They were generated during a simulation with pressure-time profile kal1 (see figures 5.5a and 5.2).

The commencement of the press step during the filling mode is recognisable in the surface representing the interaggregate porosity ε_1 and the line that forms its boundary, starting at 0.2 on $x = 0$ cm and ending at 0.4 on $x = 1.85$ cm in figure 5.6a. The line has the shape of an error function that is typical for solutions of a diffusion equation. At $t_{\text{fill}} = 0.3$ min, the value of e_1 is a little lower than its initial value of $1 - s_1^{rcp} = 0.41$ (see equation 5.4), throughout the whole cake. Via equations 2.1-2.5, 2.7, 2.31 and 3.18, it can be interpreted as the moment that the solid pressure has fully penetrated the filter cake. Typically this penetration time is $\sim L_0^2/\pi C_{e0} = 0.2$ min.

Even though aggregate oil is released near the cloth, the fraction $s_1\varepsilon_2$, which is proportional to the height of the middle surface, increases in the initial stage (of the simulated part) of the filling mode. This is due to interaggregate oil leaving the filter chamber faster than aggregate oil can flow to the interaggregate volume. Still, the line separating the top two surfaces ($s_1 \cdot \varepsilon_2$ and $s_1 \cdot s_2$), i.e. $1 - SFC$, inherits the error function shape through equations 3.31 and 3.32.

The interaggregate oil near the cloth is the first oil to flow out of the filter chamber and this head start causes the filter cake to be dryer near the cloth. The error function shape of $1 - SFC$ is maintained during the rest mode, as the gradients in e_1 decrease, and flattens a bit in the pressing mode.

The decrease of filter cake thickness can be observed through the position of the piston. The piston displacement is relatively large in the filling mode, and relatively small in the pressing mode as the filter cake becomes more stiff (elastic modulus increases, see equation 3.20) and permeability decreases (see equations 3.17 and 3.25).

During the rest mode ε_1 obtains an s-shape due to Neumann boundary conditions on both sides. At the end of the pressing mode, ε_1 smooths out completely, indicating that the filter cake has obtained a state of equilibrium. This seems to be in accordance with experiment as it was observed that oil outflow stops at the end of the process.

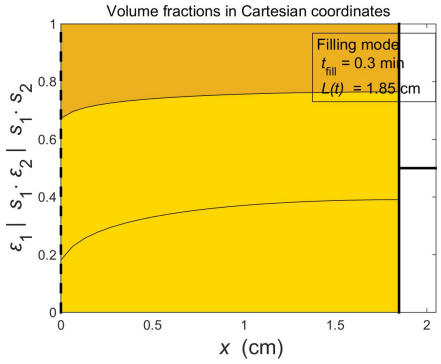

(a) Start of press step in filling mode.

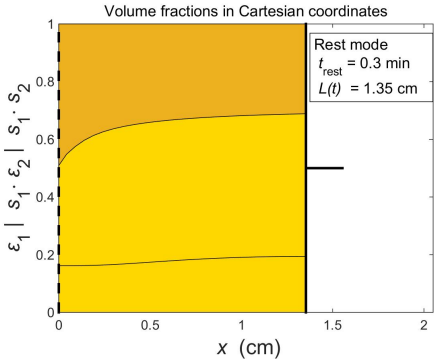

(b) The beginning of the rest mode.

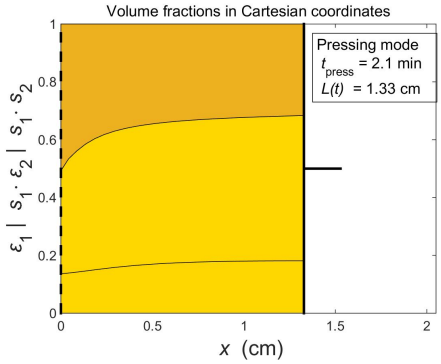

(c) First porosity drop in the pressing mode.

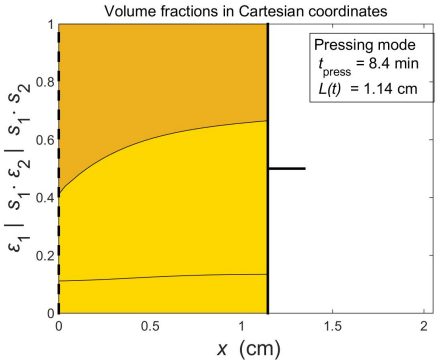

(d) Late stage of the pressing mode.

Figure 5.6: Volume fractions, shown as surfaces, at particular moments in the three modes of operation of the membrane filter press. On the horizontal axis the filter chamber location as measured from the filter cloth. t_{fill}, t_{rest} and t_{press} denote the time passed after the start of the filling, rest and pressing mode respectively.

5.1.4. VALIDATION OF THE MODEL

In this subsection, the results of the validation are presented. The validation with respect to outflow velocity is followed by a comparison of simulation with experiment regarding eventual *SFCs*. The validation that concludes this subsection is one with respect to eventual *SFC* of separate cake layers.

VALIDATION WITH RESPECT TO OUTFLOW VELOCITY

For the purpose of validation, simulations are compared to five other experiments (see table 5.1. Two experiments *ptp1a* and *ptp1b* where done with the same pressure-time profile.

Apart from *ptp2* with $R^2 = 0.80$ (figure 5.7), the agreement between simulated and experimental outflow velocities is poor. Especially in the experimental profiles that contain three maxima (caused by the three steps in the pressure-time profile): *ptp1a*, *ptp1b*, *ptp3* and *ptp4*, where the first maximum is not observed in the simulations. This is thought to be due to an overestimated $SFC_{0,P}$-value. When the $SFC_{0,P}$-value is overestimated, the

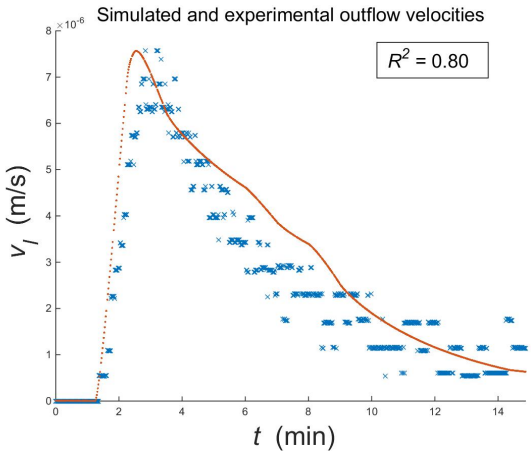

Figure 5.7: Validation with pressure time profile ptp2.

minimum pressure to squeeze the filter cake is overestimated. This minimum pressure was discussed in the last part of subsection 3.6.1. The result is that in the first step of the pressure-time profile, the minimum pressure is not reached. This in turn results in the absence of oil outflow and hence, no outflow velocity maximum can be recorded in the simulation.
The outflow velocities of the simulations of *ptp1a*, *ptp1b* and *ptp3* seem to be shifted to the right compared to the experimental curves. This is thought to arise from the delay in the measurements, which was already touched upon in the beginning of section 5.1. This delay is due to the oil having to travel through the tubes and pipes first, before arriving on the balance to be weighed.
Comparing the experiments of *ptp1a* and *ptp1b*, which were executed with the same targeted pressure profile, one can see a difference of $2 \cdot 10^{-6}$ m/s in the maximum outflow velocity. This reflects that there is substantial uncertainty in the values obtained from measurements. This uncertainty makes a proper validation difficult. Furthermore, sensitivity of the balance is an issue: the experimental outflow velocity of *ptp4* suffers from a low signal-to-noise ratio.

Nevertheless, the behaviour of the model is good qualitatively, mirroring constant acceleration in the beginning, and maxima followed by an exponential decay during retardation.

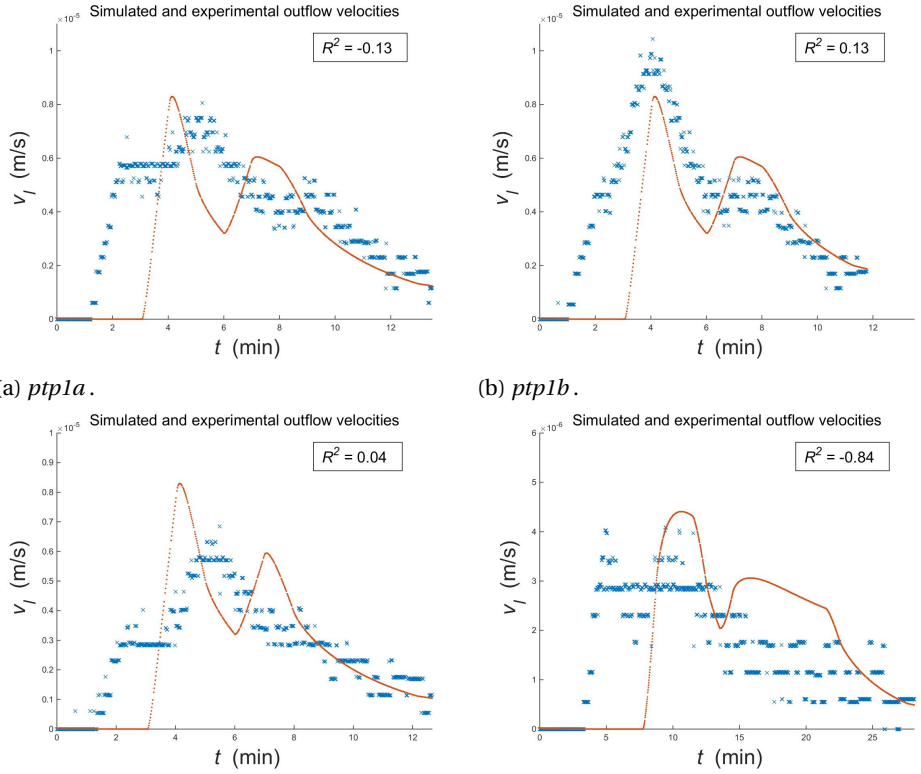

(a) *ptp1a* .

(b) *ptp1b* .

(c) *ptp3* .

(d) *ptp4* .

Figure 5.8: Validation for three more pressure-time profiles: *ptp1(a/b)* , *ptp3* and *ptp4* . The targeted pressure-time profiles for figures 5.8a and 5.8b are the same.

VALIDATION WITH RESPECT TO EVENTUAL *SFC*

Besides outflow velocities, the eventual *SFCs* are compared (see figure 5.9). For the error bars of the experiments the difference between the two experiments of *ptp1a* and *ptp1b* are taken as a measure. The error bars of the simulations are based upon the difference between eventual *SFCs* generated with the simulations of figures 5.3 and 5.5a i.e. with two different sets of calibration coefficients that capture the typical variance associated with the model.

The results of the simulation seem to be in agreement with experiment. The uncertainties, especially of the experiments, are rather large though. This was partly caused by the pressure-time profiles being controlled manually. There is a tendency for the experiments to have a higher eventual *SFC* , this is the case in five out of seven pressure profiles. As anticipated in the beginning of section 5.1, the cause might be that the oil that is still in the tubes and pipes of the filter press is not recorded in the experimental outflow velocity, with which the model is calibrated. This leads to an underestimation of the simulated eventual *SFC* .

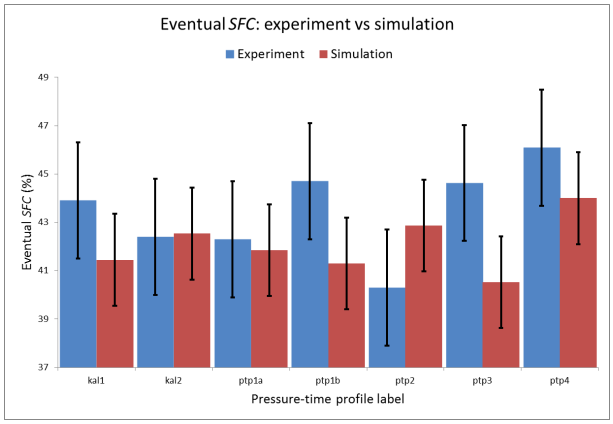

Figure 5.9: Eventual *SFCs* compared between experiment and simulation for different pressure-time profiles[44]: All are in agreement with each other.

VALIDATION WITH RESPECT TO EVENTUAL *SFC* OF CAKE LAYERS

During the experiment with pressure-time profile kal2, the filter cake that was produced in the pilot plant, was sliced into five layers of approximately the same thickness. This was done for ten samples of the filter cake. Of every cake layer, the eventual *SFC* was measured and per layer the average was taken from the ten samples. After the simulation with pressure-time profile kal2, the cake was divided into five equally thick cake layers and the average eventual *SFC* per cake layer was computed from the eventual *SFC* as function of ω^j.

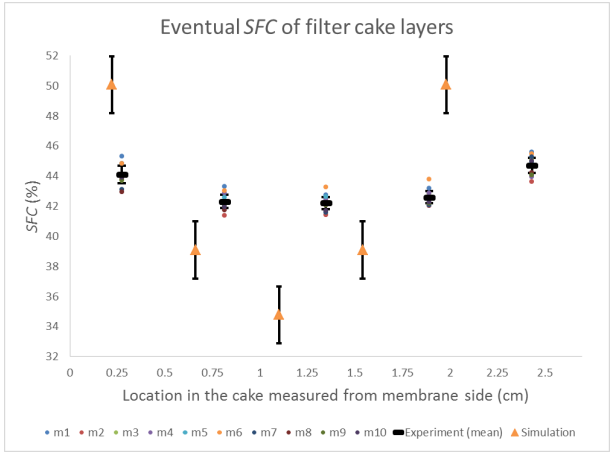

Figure 5.10: Eventual *SFCs* of five cake layers compared between experiment and simulation, both generated with the pressure-time profile kal2. The *m1 - m10* indicate the measurements of ten samples that were taken from one filter cake that was produced in the pilot plant.

Both results, from simulation and experiment, are depicted in figure 5.10. Eventual *SFC* is plotted against filter cake location as measured from the membrane side. The locations of the values in the graph correspond to the locations of the middle points of the cake layers. The uncertainties for the simulation are the same that were used in the previous subsection (see figure 5.9). The uncertainties of the experiments are 95 % confidence intervals based on the ten measurements for this particular cake (it does not show the uncertainty due to the appliance of the pressure-time profile as in figure 5.9) Uncertainties in the x-direction are not taken into account.

From figure 5.9, it could already be noted that for this pressure profile the average eventual *SFC* shows good agreement. However, in the more detailed version, it can be observed that eventual *SFC* gradients in the simulation are larger than in the experiment. Furthermore, eventual *SFC* values of separate layers do not show agreement.
In the simulation, the gradients in the interaggregate void ratio disappear eventually (see figure 5.6). Therefore, the origin of the *SFC* gradient lies in the behaviour of the aggregate oil. From equations 3.13 and 3.15, it can be deduced that the parabolic shape of the eventual *SFC* versus cake location graph emanates from the pressure gradient that has higher time-averaged values near the filter cloth.
Qualitatively, there is agreement as both the simulated and the experimental graph have this parabolic shape.
The thickness of the simulated filter cake is smaller than the filter cake from the experiment. Because the simulated average eventual *SFC* is higher than the corresponding value obtained from the experiment, this can be expected.

5.2. EFFECT OF RATE OF PRESSURE INCREASE (RPI)

The model has shown the potential to qualitatively predict the outcomes of pressure filtration under a certain pressure-time profile.In this section it is used to study differences in performance of the most basic pressure-time profiles. These profiles only contain a linearly increasing pressure followed by a constant pressure which is held until pressing mode duration reaches 30 minutes, as shown in figure 5.11. One should be careful to use these figures and the fits constructed from it as the model is not validated quantitatively. The results given here are intended to give an idea of the qualitative behaviour during the pressing mode in pressure filtration of milk fat. Results are also drawn from the model to show its possible application in process optimisation and design.

Figure 5.12 shows the *SFC* as function of time for the pressure profiles shown in figure 5.11. Almost being a mirror image of figure 5.12, figure 5.13 confirms that the origin of a large eventual *SFC* is the low amount of oil being left in the aggregates. The aggregate void ratio e_2 is a measure of this as it is the aggregate oil volume $s_1\varepsilon_2 \cdot V$ per solid fat volume $s_1 s_2 \cdot V$, the latter being constant in time according to equation 2.9. From equations 3.31 and 3.32 it follows that the evolution of e_2 is dependent on the gradient in e_1. If the RPI is lower, the longer it takes for the gradients in e_1 to vanish and for the filter cake to obtain a state of equilibrium. Therefore, it follows from equations 3.31 and 3.32 that the aggregates have more time to be squeezed out, which in turn leads to a larger eventual *SFC*.

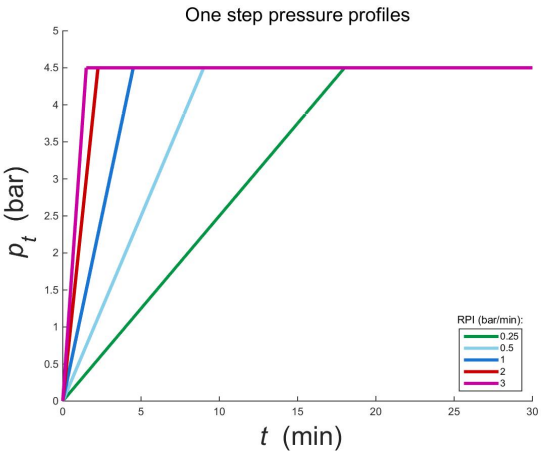

Figure 5.11: One-step pressure-time profiles used to study the effect of rates of pressure increase on eventual *SFC*.

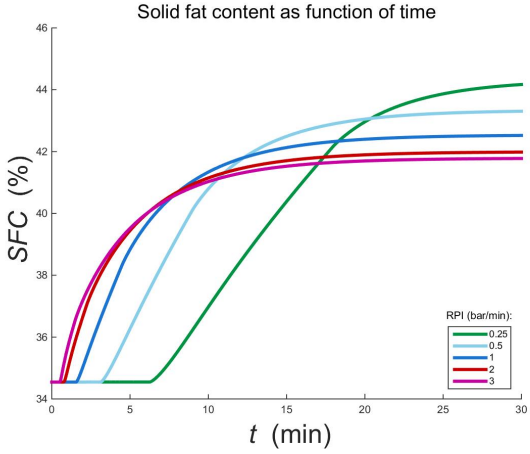

Figure 5.12: Simulated solid fat content as a function of time for the pressure-time profiles in figure 5.11.

It takes a few minutes for the *SFC* to start increasing, the exact time depending on the RPI of the OSPP. This delay is caused by the existence of a minimum pressure that needs to be reached to squeeze out the filter cake in the pressing mode. The minimum pressure is associated with the boundary value of the interaggregate void ratio after the rest mode, as pointed out in the concluding part in subsection 3.6.1.

Another graph that can be constructed from figure 5.12 shows the time required to reach a certain eventual *SFC* (figure 5.15). Like figure 5.14, it can be used to make decisions re-

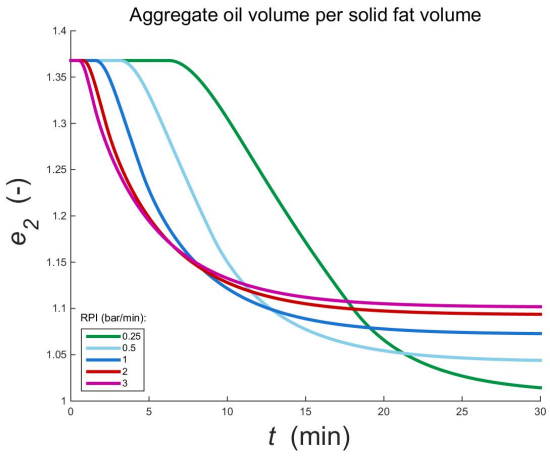

Figure 5.13: The simulated evolution of the aggregate oil in the filter cake for the pressure profiles in figure 5.11.

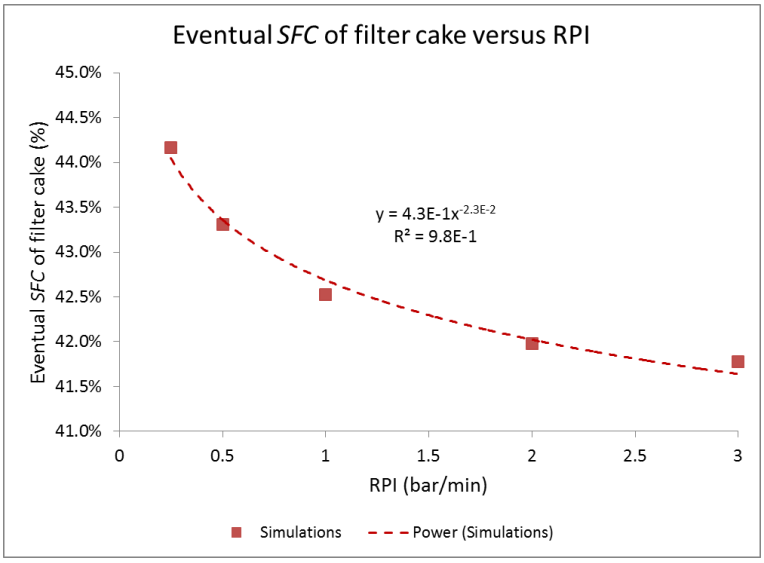

Figure 5.14: Solid fat content as a function of rate of pressure increase in the one-step pressure-time profile.

garding process optimisation and design. The trend is that the higher the desired eventual *SFC* is, the more time the pressing mode takes. Although firm quantitative conclusions cannot be drawn, from this graph it would follow that increasing the eventual *SFC* from 41.8 to 44.2 % would increase pressing mode duration by almost 50 %.

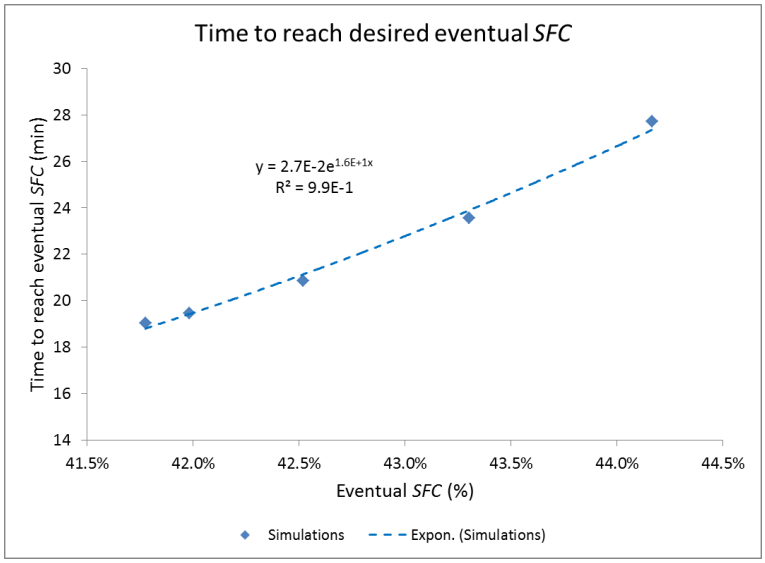

Figure 5.15: Time to reach to within 0.1 % of desired eventual *SFC* (in the pressing mode) versus eventual *SFC*: simulations and trend line

5.3. ONE-STEP VERSUS TWO-STEP PRESSURE PROFILES

The basic OSPPs can be extended adding one layer of complexity to arrive at two-step pressure-time profiles (TSPP), of which one example is shown in figure 5.16. To facilitate proper comparison to an OSPP, it is important to compare it with an OSPP with the same average RPI i.e. the same starting pressure and the same pressure after pressure increase. A second precondition for good comparison is that the time averaged pressure of both pressure profiles is the same. This is identical to stating that the areas under the $p_t(t)$-graphs have to be equal. For the pressure profiles in figure 5.16 these preconditions are met. Here, a TSPP with steps of 1 bar/min and an average RPI during the steps of 0.25 bar/min is depicted next to an 0.25 bar/min OSPP. To allow for good comparison, both pressure profiles start at the minimum pressure required to squeeze out oil from the filter cake after the rest mode as discussed in sections 3.6 and 5.2.

Results from comparisons with an 0.25 bar/min OSPP can be seen in figure 5.16. Immediately, it is clear from figure 5.17, that the OSPP delivers the largest eventual *SFC*. The TSPPs follow according to step RPI: the lower the step RPI, the higher the eventual *SFC* reached. The difference between the 0.25 bar/min OSPP and the 3 bar/min TSPP is just over 1 % in eventual *SFC*. The reasoning here is along the same lines as in section 5.2: figure 5.18 confirms a high eventual *SFC* due to more oil flowing out of the aggregates. A higher RPI allows less time for the aggregates to be squeezed out as the filter cake reaches an (temporary) equilibrium typically after two minutes. This in turn leads to a higher eventual *SFC*.

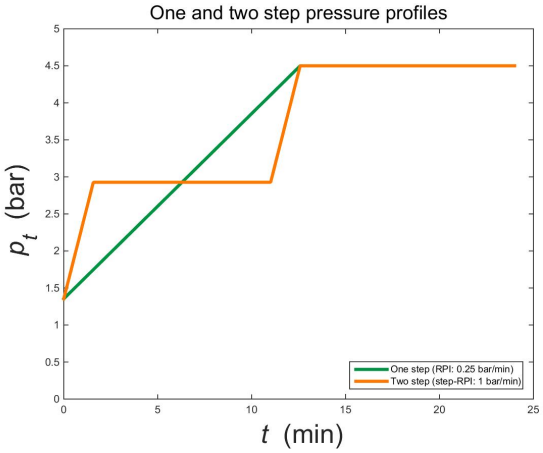

Figure 5.16: A one-step and a two-step pressure-time profile, both with the same time-averaged rate of pressure increase of 0.25 bar/min.

Observing figure 5.17, it would be interesting to see the result for the case where the second precondition for proper comparison is dropped, which states that the time-averaged pressure has to be identical. In figure 5.17 at $t \approx 7.5$ min, all TSPPs intersect with the 0.25 bar/min OSPP. One could choose a pressure profile starting like the TSPPs shown in figure 5.16, which at the intersection of the pressure profile at $t \approx 6$ min starts following the OSPP instead, i.e. a *strictly leading two-step pressure-time profile* . This should result in a higher eventual *SFC* , or at least result in obtaining higher *SFC* values more rapidly.

If the average RPI and the RPI of the OSPP is increased to for example 0.75 bar/min (see figure 5.19), the differences prove to be negligible. This stems from the fact that when comparing to a 0.75 bar/min OSPP the differences with the TSPPs in temporal time-averaged applied pressures (i.e. the areas between the profiles) are smaller than for the 0.25 bar/min OSPP case. If the difference in temporal time-averaged applied pressure is taken as a measure for the difference in pressure history, this shows that pressure history plays a role in pressure profile performance.
Although differences are small, focussing on part of figure 5.19, it shows that the model is capable of displaying complex behaviour. This is depicted in figure 5.20. In the case of the 0.75 bar/min OSPP it is not the OSPP that outperforms the TSPPs. The 1 bar/min TSPP yields the highest eventual *SFC* followed by the 2 bar/min TSPP. Similar results were obtained in comparisons with a 0.5 bar/min OSPP. It is thought to arise from the gradient in e_1 which can be larger with a larger RPI and that this has a more profound effect when the steps take less time.

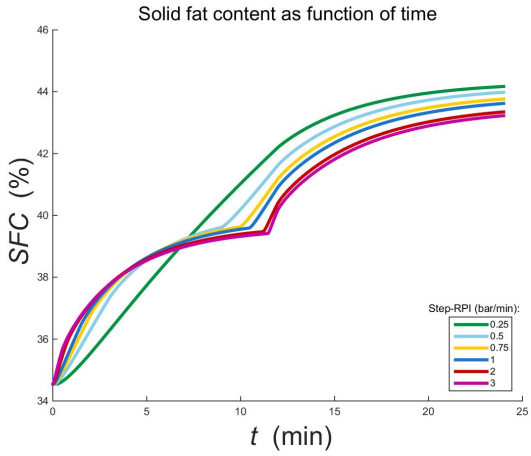

Figure 5.17: Time evolution of SFC for TSPPs with step rates of pressure increase ranging from 0.5 to 3 bar/min, compared to the 0.25 bar/min OSPP.

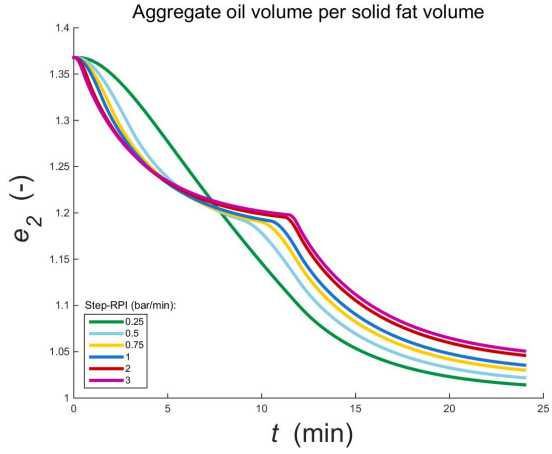

Figure 5.18: Aggregate void ratio as function of time for TSPPs with step rates of pressure increase ranging from 0.5 to 3 bar/min, compared to the 0.25 bar/min OSPP.

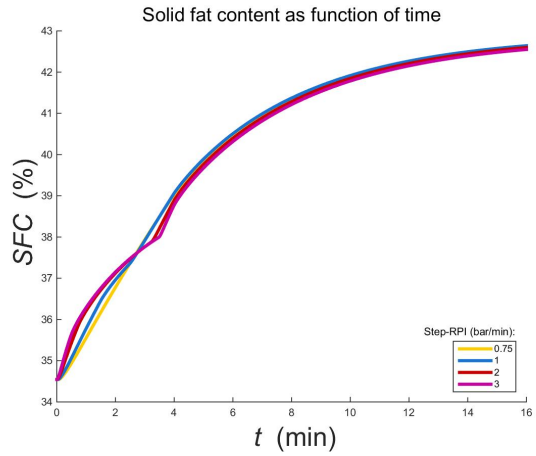

Figure 5.19: Solid fat content as function of time for TSPPs with step rates of pressure increase ranging from 1 to 3 bar/min, compared to the 0.75 bar/min OSPP.

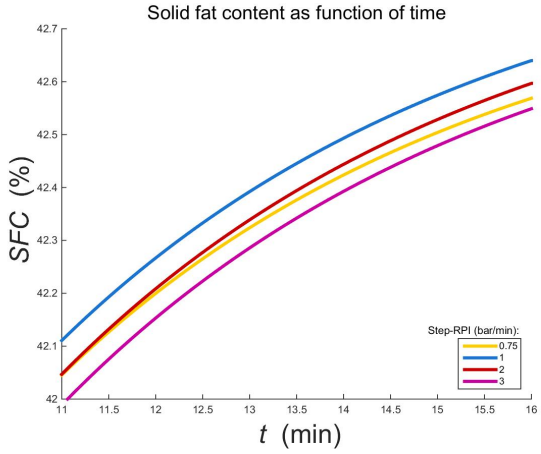

Figure 5.20: Close-up of the top right part of the graph in figure 5.19

6

CONCLUSIONS AND RECOMMENDATIONS

In the introduction of this thesis, goals and research questions were formulated. In this concluding chapter each of them will be revisited before giving recommendations for further research.

6.1. CONCLUSIONS

Starting with the first goal that was announced in the introduction:

- **Goal I**: To develop a pressure filtration model and to write the computer code to perform numerical simulations.

A pressure filtration model focussing on the press step has been developed. In short, it is a rheological model composed of two dashpots in series, which are parallel to a spring. The double porous nature of the milk fat crystal aggregate filter cake is represented by the two dashpots, which are described by a relation established by Meyer & Smith, which is an alternative to the Kozeny-Carman relation. The spring is described by an elastic modulus that was determined experimentally with a constant load test.
The model was successfully numerically implemented writing the computer code in MATLAB, from scratch. A numerical algorithm was found to successfully resolve the behaviour near the cloth boundary.
The model is capable of displaying porosities and solidosities as function of time and filter chamber location. This makes it possible to compare it with solid fat contents *(SFCs)* of different cake layers retrieved from experiment. It can also generate graphs with oil outflow velocity, filter cake *SFC* and aggregate oil volume as function of time. It is possible, to do this analysis for different pressure-time profiles. This allows a comparison between pressure-time profiles to select one that obtains a better separation and consequently, a dryer filter cake. The model provides a guidance in the search for values of different parameters through specific tests.

In the process of creating the model and in the evaluation of its performance compared to experiments, the model has given valuable insights and understanding regarding the role of numerous parameters.

- **Goal II**: To validate the pressure filtration model.

Simulations with the pressure filtration model have been compared to experiments to contrast outcomes regarding oil outflow velocity, eventual *SFC* and eventual *SFC* of different cake layers. This has lead to the conclusion that quantitatively, the model could not be validated. However, qualitatively, the model has been validated or at least has shown the potential to be qualitatively valid.

- **Goal III**: To perform simulations to gain insight into critical factors that lead to a higher olein yield.

Computer simulations have been performed to investigate the effect of different pressure-time profiles. The time-averaged RPI (rate of pressure increase) has been found to be a critical factor to attain a higher *SFC* in the stearin fraction (S fraction) and simultaneously obtain a higher olein yield.
The addition of a step in the two-step pressure profiles (TSPPs) has been observed not to be a critical factor for olein yield.

- **Question I**: Is it favourable to apply a high rate of pressure increase in the pressure-time profile during the expression of anhydrous milk fat (AMF)?

No, it is not preferred to have a high RPI. The contrary has been found in section 5.2: a simulation with the 0.25 bar/min one-step pressure profile (OSPP) resulted in the highest eventual *SFC* (and thus the highest olein yield) of the OSPPs simulated. It was found that the higher the RPI is, the lower the eventual *SFC* attained. The longer it takes for the filter cake to reach a state of equilibrium, the more time the aggregates have to release their oil. Hence, it is favourable to apply a low RPI.

- **Question II**: Given a certain rate of pressure increase, does a linear one-step pressure-time profile give the highest eventual *SFC*?

It depends. For a time-average RPI of 0.25 bar/min the linear OSPP gives the best result, when compared to TSPPs with the same time-averaged applied piston pressure. The difference in eventual *SFC* was observed in section 5.3 to be in the order of 1 %.
For a time-average RPI of 0.5 and 0.75 bar/min, the differences between OSPP and TSPP are negligible (if time-averaged applied piston pressures are equal).

Main conclusion from this research is that a lower RPI yields a higher eventual *SFC* and thus yields a better result. The question for the process technologist is whether it is worth taking the extra time to reach this *SFC* (see figure 5.15).

6.2. RECOMMENDATIONS

One of the problems in the validation is the large uncertainty in the measurements obtained in experiments. Conducting more experiments will lead to decreased uncertainties in outflow velocities and *SFC* outcomes measured. This also allows for a calibration with one pressure profile with less uncertainty or with more different pressure profiles, so that the calibration is less sensitive to the uncertainties in the experiments. During experiments it is also advised to use a balance that is more sensitive and is able to make measurements at a higher frequency. This should result in an outflow velocity signal which contains less noise.
Experiments with a compression cell under similar conditions as that of the membrane filter press might solve the problem with the delay associated with the oil travelling from cloth to balance.

Furthermore, within the model some components could be critically reassessed. Is the method for establishing the experimental relation for the elastic modulus valid within the context of the present model? Is the use of only one elastic modulus enough when modelling a double porous filter cake? Various other rheological models can be tested and compared to the one presented in this thesis to study whether it improves predictions.
The relatively high gradients in simulated eventual *SFC* suggest that a model where the interaggregate oil production is dependent on solid pressure could be an alternative worth investigating.

With the current model it would be interesting to research whether strictly leading two-step pressure profiles can produce S fractions with a higher *SFC*.
Only 24 nodes were used and therefore, simulation duration was not substantial (3 minutes per simulation). However, during a calibration this can add up to a large time span. Implementation of a non-equidistant grid and a variable time step would allow for faster computation while maintaining the same level of accuracy.
Since the differences between OSPPs and TSPPs are small, it is expected that other multistep pressure profiles also yield small differences, even more so because under preconditions mentioned in section 5.3 a multistep pressure profile with n steps converges to an OSPP when $n \to \infty$. This expectation can be verified in future research.

NOMENCLATURE

ROMAN SYMBOLS

Symbol	Description	Units	Equation of introduction
a	Aggregate area per volume	m^{-1}	3.15
a_1	Flow resistance factor for interaggregate volume	-	-
a_2	Flow resistance factor for aggregate volume	-	-
c_1	Fit coefficient	Pa	3.18
c_2	Fit coefficient	-	3.18
C_{e0}	Overestimation of c_{e_1}	m^2/s	4.1
c_{e_1}	Consolidation coefficient maximum	m^2/s	3.21
$C_e(e_1, e_2)$	Consolidation coefficient	m^2/s	3.23
c_q	Constant for production q	m/s	3.28
$\frac{D^s}{Dt}$	Solid phase material derivative	s^{-1}	2.16
d_c	Characteristic diameter of the crystals	m	3.25
d_p	Aggregate diameter	m	2.19
dR	Local flow resistance	m^{-1}	2.25
$d\omega$	Infinitesimal 1D solid volume	m	2.11
$E(\varepsilon_{ls})$	Elastic modulus	Pa	2.32
e	Total void ratio	-	2.7
e_0	Total void ratio at random close packing	-	2.31
e_1	Interaggregate void ratio	-	2.6
$e_1^{i,j}$	Interaggregate void ratio at time step i and grid position j	-	4.6
$e_1^{\Gamma_1}$	Interaggregate void ratio at cloth boundary	-	3.38

Symbol	Description	Units	Equation of introduction
e_2	Aggregate void ratio	-	2.6
$e_2^{\Gamma_1}$	Aggregate void ratio at cloth boundary	-	3.38
$e_2^{\Gamma_2}$	Aggregate void ratio at piston boundary	-	-
$e^{i,j}$	Total void ratio at time step i and grid position j	-	4.19
e^{Γ_1}	Total void ratio at cloth boundary	-	3.37
$e_2^{i,j}$	Aggregate void ratio at time step i and grid position j	-	4.10
F_d	Drag force per unit volume	N/m^3	2.16
$f(e_2)$	Substitution function for equation 4.3	-	4.4
$f^{i,j}$	Discrete $f(e_2)$ at time step i and grid position j	-	4.8
Fo_Δ	Local Fourier number	-	4.1
g	Gravitational acceleration	m/s^2	2.16
$\vec{g}$	Gravitational acceleration	m/s^2	2.18
$g(e_1, e_2)$	Substitution function for equation 4.3	-	4.4
$g^{i,j}$	Discrete $g(e_1, e_2)$ at time step i and grid position j	-	4.8
J	Number of length segments between nodes	-	-
j	Index denoting grid position	-	4.6
k	Permeability	m^2	2.21
k_p	Multiplication factor for pressure profile during filling	-	-
L	Length of filter cake/chamber	m	2.26
L_0	Initial (equivalent) filter cake thickness	m	-
L^i	Filter cake length at time step i	m	5.2
L_y	Width of the filter chamber	m	-
L_z	Height of the filter chamber	m	-
p_l	Liquid pressure	Pa	2.18
p_p^i	Piston pressure at time step i	Pa	4.18

Symbol	Description	Units	Equation of introduction
$p_p(t)$	Over pressure applied by piston	Pa	3.35
p_s	Solid pressure	Pa	2.17
q	Production of interaggregate oil	s^{-1}	3.1
$q^{i,j}$	Discrete q at time step i and grid position j	s^{-1}	4.9
R^2	Coefficient of determination	-	-
Re_h	Reynolds number based on hydraulic diameter	-	2.19
R_d	Flow resistance of cloth	m^{-1}	3.34
R_k	Total flow resistance of filter cake	m^{-1}	
R_k^i	Discrete R_k at time step i	m^{-1}	4.18
s	Total solidosity (solid fat volume fraction)	-	2.5
$s_{0,P}$	Solid fat volume fraction at start of pressing mode	-	-
s_1	Interaggregate solidosity	-	2.4
s_1^{hcp}	Maximum close packing fraction (solidosity)	-	-
s_1^{rcp}	Random close packing fraction (solidosity)	-	-
s_2	Aggregate solidosity	-	2.4
SFC	Solid fat content	-	5.1
$SFC_{0,P}$	Solid fat content at start of pressing mode	-	-
s^{rcp}	Solid fat volume fraction at random close packing	-	3.43
t	Time	s	2.8
t_{fill}	Time passed after start of filling mode	s	(figure 5.6)
t^i	Index denoting time step	s	4.6
t_{press}	Time passed after start of pressing mode	s	(figure 5.6)
t_{rest}	Time passed after start of rest mode	s	(figure 5.6)
V	Filter cake volume	m^3	-
V_p	Typical pore volume	m^3	-
$\vec{v}_l$	Velocity of the liquid	m/s	2.12
$\vec{v}_{l,2}$	Velocity of the aggregate oil	m/s	3.11
$v_{l_2,x}$	The x-component of $\vec{v}_{l,2}$	m/s	3.12

Symbol	Description	Units	Equation of introduction
$v_{l,a\rightarrow ia}$	Oil flux through aggregate surface	m/s	3.15
v_l^i	Outflow velocity at time step i	m/s	5.2
$\vec{v}_s$	Velocity of the solid phase	m/s	2.8
$v_{s,x}$	The x-component of $\vec{v}_s$	m/s	2.16
v_σ	Superficial velocity	m/s	2.15
v_{σ_2}	Superficial velocity of aggregate oil	m/s	3.12
w_R^j	Weighting factor defined in equation 4.21	-	4.20
x	Filter chamber location, Cartesian coordinate	m	-

GREEK SYMBOLS

Symbol	Description	Units	Equation of introduction
Γ_1	Cloth boundary	-	-
Γ_2	Piston boundary	-	-
$\Delta e_1^{i,j}$	Difference between interaggregate void ratios at time step i and grid position j	-	4.24
Δp_d	Pressure drop over cloth	Pa	3.34
Δp_k	Pressure drop over the whole cake	Pa	2.24
Δp_k^i	Discrete Δp_k at time step i	Pa	4.18
Δp_t	Total pressure drop over the domain	Pa	3.34
Δt	Size of time step	s	4.6
$\Delta\omega$	Distance between two nodes in grid	m	4.1
$\delta V(t)$	Total volume of fragment of filter cake	m^3	2.1
δV_a	Aggregate volume	m^3	2.1
δV_{ap}	Aggregate pore volume	m^3	2.2
δV_{ia}	Interaggregate volume	m^3	2.1

Symbol	Description	Units	Equation of introduction
δV_s	Solid fat volume	m^3	2.2
$\delta x(t)$	Thickness of filter cake element	m	2.10
δx_u	Thickness of filter cake slice before deformation	m	2.30
δy	Width of filter cake element	m	-
δz	Height of filter cake element	m	-
ε_1	Interaggregate porosity	-	2.3
ε_1^{rcp}	Porosity at random close packing	-	-
ε_2	Aggregate porosity	-	2.3
ε_{ls}	logarithmic strain	-	2.30
$\varepsilon_{ls}^{i,j}$	Strain at time step i and grid position j	-	4.18
$\varepsilon_{ls}^{\Gamma_1}$	Logarithmic strain at cloth boundary	-	3.36
μ	Viscosity of oil	$Pa \cdot s$	2.18
ρ_l	Density of the liquid	kg/m^3	2.12
ρ_s	Density of the solid phase	kg/m^3	2.8
τ_{xx}	Principal stress in the x-direction	Pa	2.16
Ω	1D solid volume of filter cake/chamber	m	-
ω	Filter chamber location, material coordinate	m	-
ω^j	Discrete material coordinate	m	-

ABBREVIATIONS

Abbreviation	Word/phrase
AMF	Anhydrous milk fat
kal	Calibration pressure-time profile
NMR	Nuclear magnetic resonance
O	Olein
OSPP	One-step pressure-time profile
ptp	Pressure-time profile
RPI	Rate of pressure increase
S	Stearin
SFC	Solid fat content
TSPP	Two-step pressure-time profile

ACKNOWLEDGEMENTS

Although this is not a study on *blood, sweat and tears* flow, it surely was a demonstration of it. At least, the last bits of work finishing the report took quite some effort. To put it in the words of the first sentences of the introduction:

It was I who performed the sacrifice,
filtered the clarified butter,
and collected the olein,
and I made it into,
a readable thesis.

This thesis, forms the end of my study in Delft, a long journey which might be reflected on as a detour. And even though the detour sparked joy, there were times where a little bit more effort, dare and direction would have paid off. When you think of it, the trademark *just do it* is actually not a bad motto. I will take that as a valuable lesson learned, amongst many other insights. And, in the end, contrary to some of other people's convictions, I did it! And, this accomplishment, will be the starting point for a bright and productive future!

I could not have done this master thesis project without the help of Harrie van den Akker. It was a very short first scheduled meeting, standing in the hallway of the Transport Phenomena group. He did not hesitate to take me aboard and for that I am thankful. Despite the fact that he is a full-time professor in Limerick, Ireland, he has been here to guide me, to discuss the workings of the model, to pose critical questions about my work and even to go to Wageningen together.
It was fun to discuss the topics of industry and academia whilst sitting in the comfortable seat of your *MG* . Your work ethic and continuous positive spirit are admirable.
In Wageningen, we would have the monthly update about the project, as this was an assignment that had been created at FrieslandCampina by William Kloek. The assignment was originally pitched at a workshop called *Physics of Industry* . It was at this workshop that Harrie and William met. The report, that was a result of that intense week, was a starting point for this research. I have to thank William for giving me the chance to work with him and FrieslandCampina. In the middle of my master project, I was accepted to do the experimental work as part of an internship at FrieslandCampina in Wageningen. My first real experience with professional business was a very good one! Also due to the nice colleagues. Johan Draisma showed me around in the plant in Noordwijk, Groningen, where the membrane filter press was in full operation. Richard van Leeuwen helped me with the day-to-day business and occasionally both of them would join for the monthly update meeting. Being allowed to work in the pilot plant and to use all the valuable laboratory equipment was magnificent! Hanung, thank you for assisting me.

William, I want to thank you for your fruitful discussions and bright ideas. Are you sure a phd in physics wasn't the right thing for you to do instead? For the moment, I am sure that I will pass on a concert of deathspell solid 1D volume, I mean deathspell omega ;)

I want to thank the other committee members, Chris Kleijn and Fred Vermolen, for taking interest in my work. I am, at this moment, confident that we will have a fair and perhaps enjoyable discussion about it.

At TP, I want to thank Luis Portela, Sasja Kenjeres, Rob Mudde, Siddhartha Mukherjee and Manu Chakkingal for consultations. From other research groups I'd like to show appreciation to Fons Daalderop, Duncan van der Heul, Pouyan Boukany and Maulik Shah. And in the light of overcoming difficulties in research by taking the time of other students and explaining the problem, I have to note the valuable insights and input of Jorne Boterman (even better than Buttersack![17]), Stefan Zwinkels and Victor Oppenneer.
I cannot name all fellow students at TP, but I enjoyed coming to the hallway corner office every day to be in your company.

Thank you Sophie, my dear sister, for taking the effort to read and give feedback on part of the manuscript. Petra and Marieke, thanks for your support.
Special word of thanks goes to Jan a.k.a. Jbo. I always enjoy our constructive conversations that started with hobbel 1. Coert, mon frère, I like that we can always talk about anything and it was nice to visit the heath of Ginkel during the weekend in Wageningen.

Mom and dad, I hope you've enjoyed this thesis about the efficiency of separation. It should have been handed to you earlier.
That said, I could not have done this without you. Thank you.

Et Sylvia, merci pour d'être d'un grand soutien. J'adore célébrer le week-end avec toi mon amour, chaque week-end (et plus)! Et bien-sûr, aussi avec Eiffel: la bande est complet! Peut-on recommencer le week-end?

Doedo

BIBLIOGRAPHY

[1] E. K. Neumaier, *Readings in Eastern Religions* (Wilfrid Laurier Univ. Press, 2006) p. 7.

[2] H. McGee, *On Food and Cooking* (Scribner, 2004) p. 12.

[3] R. J. Wakeman, *Filtration* (Elsevier Advanced Technology, 1999) p. 6.

[4] *idem*, p. 213.

[5] E. J. La Heij, P. J. Kerkhof, A. Herwijn, and W. Coumans, *Fundamental aspects of sludge filtration and expression,* Water Research **30**, 697 (1996).

[6] A. D. Stickland, R. G. De Kretser, and P. J. Scales, *Nontraditional constant pressure filtration behavior,* AIChE journal **51**, 2481 (2005).

[7] Y. Hua, *Modellierung der eindimensionalen Abpressung von Zuckerrübenschnitzeln* (PhD thesis, Braunschweig Univ. of Technology, 1998) p. 1.

[8] R. E. Timms, *Fractional crystallisation–the fat modification process for the 21st century,* European journal of lipid science and technology **107**, 48 (2005).

[9] S. Rønholt, K. Mortensen, and J. C. Knudsen, *The effective factors on the structure of butter and other milk fat-based products,* Comprehensive Reviews in Food Science and Food Safety **12**, 468 (2013).

[10] E. Deffense, *Milk fat fractionation today: a review,* Journal of the American Oil Chemists' Society **70**, 1193 (1993).

[11] C. Lopez and M. Ollivon, *Triglycerides obtained by dry fractionation of milk fat: 2. thermal properties and polymorphic evolutions on heating,* Chemistry and Physics of Lipids **159**, 1 (2009).

[12] B. Ruth, *Studies in filtration III. Derivation of general filtration equations,* Industrial & Engineering Chemistry **27**, 708 (1935).

[13] P. C. Carman, *Fluid flow through granular beds,* Trans. Inst. Chem. Eng. **15**, 150 (1937).

[14] F. M. Tiller and H. Cooper, *The role of porosity in filtration: IV. Constant pressure filtration,* AIChE Journal **6**, 595 (1960).

[15] K. von Terzaghi, *Die berechnung der durchassigkeitsziffer des tones aus dem verlauf der hydrodynamischen spannungserscheinungen,* Sitzungsber. Akad. Wiss. Math. Naturwiss. Kl. Abt. 2A **132**, 105 (1923).

[16] M. Shirato, T. Murase, A. Tokunaga, and O. Yamada, *Calculations of consolidation period in expression operations,* Journal of Chemical Engineering of Japan **7**, 229 (1974).

[17] C. Buttersack, *Two-zone model for solid—liquid separation by filtration and expression,* Chemical engineering science **49**, 1145 (1994).

[18] J. Lanoisellé, E. I. Vorobyov, J. Bouvier, and G. Pair, *Modeling of solid/liquid expression for cellular materials,* AIChE Journal **7**, 2057 (1996).

[19] M. Petryk and E. Vorobiev, *Numerical and analytical modeling of solid–liquid expression from soft plant materials,* AIChE Journal **59**, 4762 (2013).

[20] G. Kamst, O. Bruinsma, and J. De Graauw, *Solid-phase creep during the expression of palm-oil filter cakes,* AIChE journal **43**, 665 (1997).

[21] G. Kamst, O. Bruinsma, and J. De Graauw, *Permeability of filter cakes of palm oil in relation to mechanical expression,* AIChE journal **43**, 673 (1997).

[22] G. S. Blair and B. Veinoglou, *A study of the firmness of soft materials based on Nutting's equation,* Journal of Scientific Instruments **21**, 149 (1944).

[23] G. Kamst, *Filtration and expression of palm oil slurries as a part of the dry fractionation process* (PhD thesis, Delft Univ. of Technology, 1995) p. 134.

[24] *idem*, p. 139.

[25] *idem*, p. 116.

[26] SOFIL s.r.l., *Filtering phases for a membrane plate filter press,* http://www.filmac-filter.com/en/filtering_process.php, [Online; accessed 25 May 2018].

[27] G. Pinder and W. Gray, *Essentials of multiphase flow and transport in porous media* (John Wiley & Sons Inc., 2008) p. 71.

[28] *idem*, p. 45.

[29] G. Kamst, *Filtration and expression of palm oil slurries as a part of the dry fractionation process* (PhD thesis, Delft Univ. of Technology, 1995) p. 31.

[30] G. Pinder and W. Gray, *Essentials of multiphase flow and transport in porous media* (John Wiley & Sons Inc., 2008) pp. 106, 107.

[31] H.E.A. Van den Akker and R.F. Mudde, *Transport Phenomena* (Delft Academic Press, 2014) p. 283.

[32] H. Brinkman, *A calculation of the viscous force exerted by a flowing fluid on a dense swarm of particles,* Flow, Turbulence and Combustion **1**, 27 (1949).

[33] J. Olivier, J. Vaxelaire, and E. Vorobiev, *Modelling of cake filtration: an overview,* Separation Science and Technology **42**, 1667 (2007).

[34] S. Torquato, T. M. Truskett, and P. G. Debenedetti, *Is random close packing of spheres well defined?* Physical review letters **84**, 2064 (2000).

[35] C. Tien and B. V. Ramarao, *Can filter cake porosity be estimated based on the Kozeny–Carman equation?* Powder technology **237**, 233 (2013).

[36] R. J. Wakeman, *Filtration* (Elsevier Advanced Technology, 1999) p. 21.

[37] B. A. Meyer and D. W. Smith, *Flow through porous media: comparison of consolidated and unconsolidated materials,* Industrial & engineering chemistry fundamentals **24**, 360 (1985).

[38] D. P. Hazelhoff Heeres, *Effect of different pressure-time profiles on milk fat filtration* (FrieslandCampina Research, internal report, 2017) p. 29.

[39] G. Kamst, *Filtration and expression of palm oil slurries as a part of the dry fractionation process* (PhD thesis, Delft Univ. of Technology, 1995) p. 117.

[40] D. P. Hazelhoff Heeres, *Effect of different pressure-time profiles on milk fat filtration* (FrieslandCampina Research, internal report, 2017) p. 20.

[41] *idem*, pp. 7–14.

[42] *idem*, p. 1.

[43] F. M. Tiller and C. Yeh, *The role of porosity in filtration. part XI: Filtration followed by expression,* AIChE journal **33**, 1241 (1987).

[44] D. P. Hazelhoff Heeres, *Effect of different pressure-time profiles on milk fat filtration* (FrieslandCampina Research, internal report, 2017) p. 43.